White paper

Automatic landmarking and parsing of human anatomy (ALPHA) for innovative and smart MI applications

Vijay Shah, Ph.D.

siemens-healthineers.com

SIEMENS Healthineers

Table of contents

Acronyms

AC_CT	Attenuation correction CT
AI	Artificial intelligence
ALPHA	Automatic landmarking and parsing of human anatomy
CT	Computed tomography
FAST	Fully assisting scanner technologies
FDG	Fluorodeoxyglucose
HL	Hodgkin lymphoma
Ki	Metabolic rate
LEAP	Learning ensembles of anatomical patterns
MI	Molecular imaging
MR	Magnetic resonance
MRFDG	(^{18}F FDG) metabolic rate
MRGlu	Glucose metabolic rate
NHL	Non-Hodgkin lymphoma
PACS	Picture archiving and communication system
PERCIST	PET response criteria in solid tumors
PET	Positron emission tomography
ROI	Region of interest
SiPM	Silicon photomultiplier
SPECT	Single photon emission computed tomography
SUV	Standardized uptake value
VD	Distribution volume
WB	Whole-body

Introduction

Over the past decades, molecular imaging (MI) has grown into a vital tool for precision medicine with potential to offer tremendous capabilities for the detection and assessment of the significance of diseases, risk stratification, therapy selection, and monitoring in oncology, cardiology, and neurology.[1] Modern MI systems are typically hybrid systems—PET/CT or SPECT/CT—that seamlessly combine the richness in anatomical images (CT) with functional images (PET and SPECT). Furthermore, technology advances in equipment, such as the introduction of silicon photomultiplier (SiPM)-based PET detector, have increased spatial resolution and sensitivity that can be utilized to obtain images of increased quality at lower radiation doses. Improvements in reconstruction algorithms, such as xSPECT™ technology, further expand the spectrum of clinical applications by incorporating CT-based tissue segmentation into a zonal image reconstruction to enable a new degree of image quality[2] as well as quantitative SPECT measurements.

In the era of value-based medicine, it has become essential to assist technologists and clinicians by reducing manual, laborious, and non-essential work to enable the efficient processing of high volumes of data in a fashion that is efficient, robust, reproducible, and less operator dependent. This will also allow them to focus their time and attention on patients and critical clinical questions. Thus, to increase throughput without sacrificing quality requires innovative, impactful features using unique intelligent technologies.

Artificial intelligence (AI)-powered algorithms impact the entire image acquisition, reconstruction, and interpretation of molecular images. Automatic landmarking and parsing of human anatomy (ALPHA), a Siemens Healthineers proprietary technology, supports optimized workflows on both scanners and *syngo*.via reading solutions. This white paper introduces ALPHA technology as well as scanner technologies and *syngo*.via features driven by ALPHA technology.

ALPHA

ALPHA[1-6] can detect and contextualize anatomical structures at various levels of anatomical abstraction, as shown in Figure 1.

Figure 1

(a)

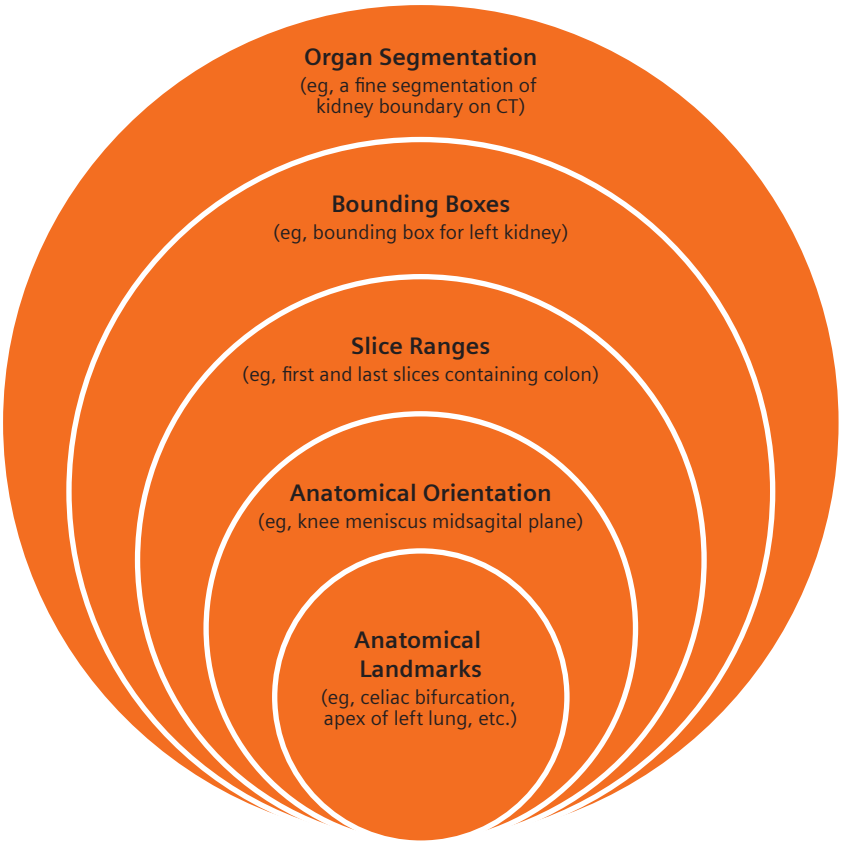

(b)

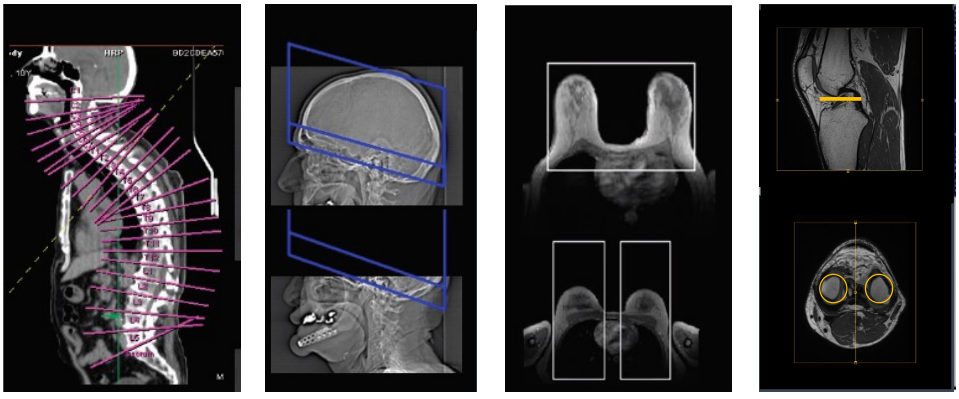

Figure 1. (a) ALPHA, example of how it works. (b) ALPHA detects various anatomical structures to assist the acquisition or reading of medical images. Several examples from left to right of the image demonstrate robustness of ALPHA technology: automatic vertebra localization and labelling performed to provide planes at C1-C7, T1-T12, L1-L5, S (abnormal patient positioning); results for head scan ranges—the lower edge should go through the canthomeatal line (works even when full anatomy is not present); detection of bounding boxes around the breast or separately for right and left breast regions on MRI images; plane alignment for optimal imaging of the menisci in MRI images.

Core idea: mimic human vision

ALPHA can be used to recognize and infer anatomical patterns and consists of an algorithm to detect anatomical landmarks at its core, as shown in Figure 1a. An anatomical landmark is a discrete labelled point in 2D or 3D medical images that can be used as a reference point by readers to identify anatomy, eg, apex of left lung or top of liver dome. The algorithm is designed to mimic the human foveal vision system, which only focuses on points of interest, for example, landmark points while perceiving a rough and blurred peripheral context at any given time. Typically, the human visual system analyzes the complete scene and use redundancy and relationships of surrounding structures to achieve a reliable recognition of objects or context. ALPHA was designed in the same way to recognize an abundant number of anatomical landmarks and structures by exploiting the rich context and high redundancy in a medical imaging. The underlying technology is a multi-layered, machine-learning algorithm called learning ensembles of anatomical patterns (LEAP).[4-5]

How ALPHA learns

ALPHA at its core has an engine to identify landmarks. The algorithm has been trained using many expert-annotated images across modalities consisting of many landmarks distributed throughout the body as shown in Figure 2. Using a statistical learning and feature selection algorithm, the engine learned to formulate a knowledge base to detect landmarks based on image features that best discriminate the target landmark appearance from the other structures.

Algorithm learning is based on training using images present in a vast database without making any explicit assumptions regarding the target anatomy or modality. This allows ALPHA to be highly scalable to different anatomical structures and to different imaging modalities (eg, CT or MRI) or appearance (eg, 2D images, 3D images, topograms). For a new image volume, a runtime engine uses the knowledge base to identify landmarks. A sample landmark detection in liver is shown in Figure 2.

Figure 2

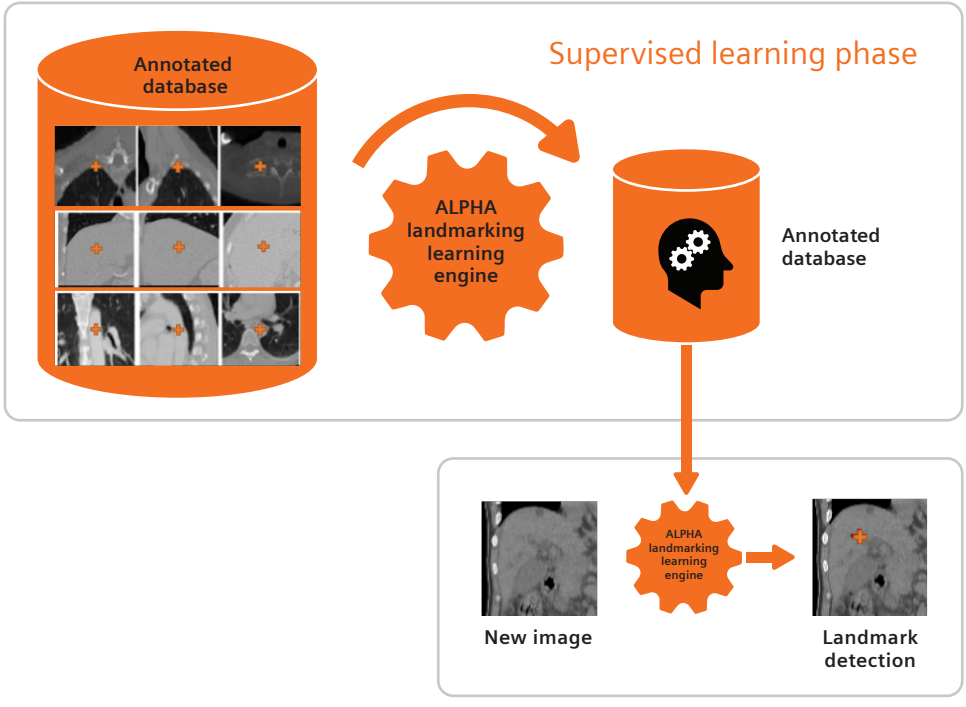

Figure 2. The supervised learning phase of the ALPHA landmarking engine. The database consists of image data annotated by expert readers. The algorithm is trained on this data to create a knowledge base that is used by the runtime engine to detect landmarks in a new image (center of liver anatomical landmark is detected).

Increase accuracy and reliability via redundancy[3]

In the presence of a visual illusion, the human brain is vulnerable to misinterpretation and 'human error;' conversely, machine learning algorithms similarly are also susceptible to misinterpretation.[7] In order to achieve robustness against diseases or imaging artifacts, ALPHA uses multiple layers of redundancy[3] to increase the reliability of the results produced by the algorithm. The concept of redundancy has been shown to work well in safety-critical systems, as failure of a single component can be either detected or corrected by other working components. ALPHA uses three redundancy concepts to achieve robustness.

1. Redundancy of training data based on anatomical landmarks

Research has shown that ensemble learning algorithms, such as bagging[6], improves performance of the system: learning is performed by selecting a few samples for training from the available training data to train multiple detectors. In contrast, ALPHA uses a spatial re-alignment scheme that uses all available training data.[3] The training data was aligned according to anatomical landmarks that were annotated by the experts as shown in Figure 3. Because of inherent anatomical variability, all landmarks cannot be aligned together. Redundancy was included by replicating the data for multiple landmarks within the body.[3-6]

Figure 3

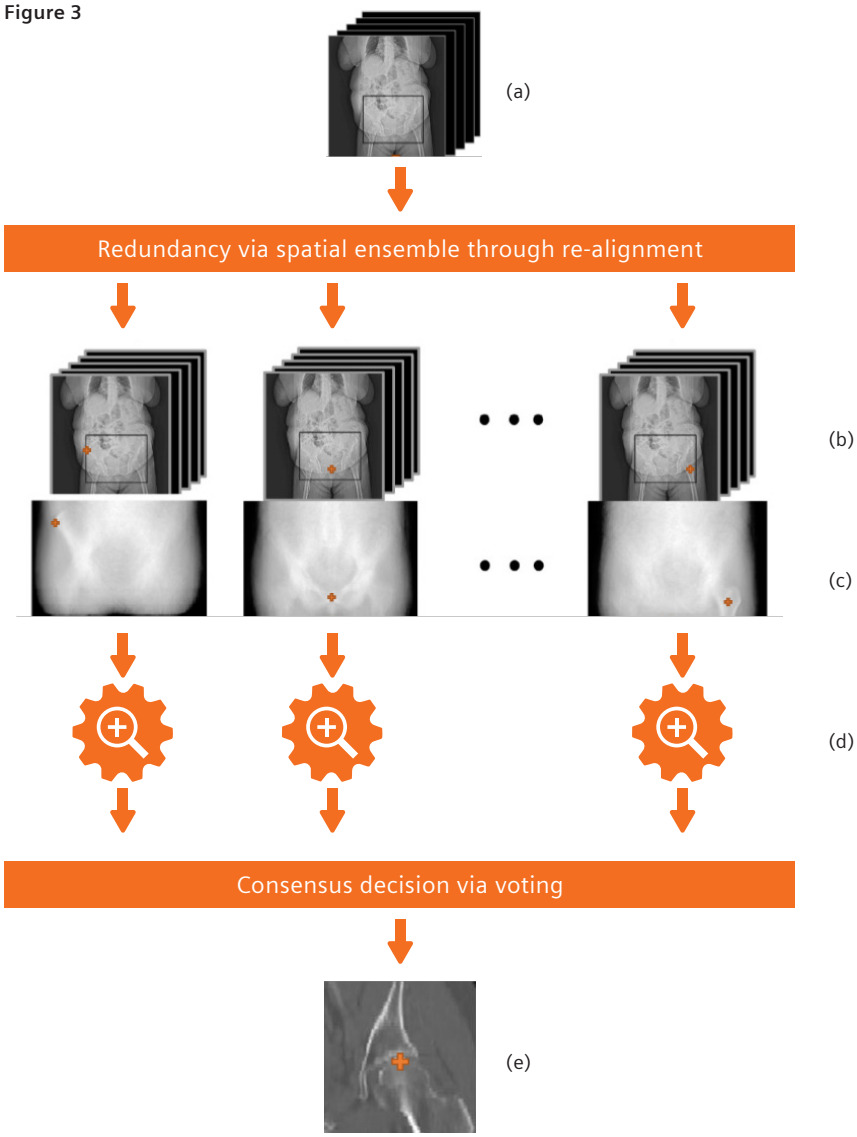

Figure 3. Spatial ensemble learning to exploit redundancies and dependencies for improved robustness. Original training data (a) is spatial ensemble through re-alignment, for example all training data is duplicated and realigned to different anatomical landmarks (b). Finally, the median value is calculated from all the training datasets (c) followed by running the landmark detection algorithm3-6 in (d). Final target prediction of the landmark (e) is performed using the consensus decision made via a voting process.

Thus, if *n*-landmarks are annotated in data, there will be n times the original data present for the training as new dataset is created by re-alignment of *n*-landmarks as shown in Figure 3b. The advantage of spatial alignment can be seen in Figure 3c, the median image, where images are much sharper in the region of landmark point and blurry at the region away from the landmark point. The detector algorithm is run separately on each of these images, creating redundant prediction of landmarks, which is then appropriately selected based on the voting scheme described later in section 3.

2. Redundancy from different voxel resolutions

Traditionally for object detection, a coarse-to-fine level search strategy is employed to improve the speed of target search. ALPHA employs a multi-scale approach to landmark detection but is optimized to the trade-off between efficiency (time to detect the landmarks) and robustness (accuracy of landmark location). To introduce redundancy, the detection performed at finer scales is not dependent on proposal obtained by detection performed at the coarser level. This allows a finer detector to search in a range as wide as allowable by the speed requirements of the application. Such a strategy can capture occasional errors, especially at finer scales. Ambiguity or contradiction can happen on medical images, for example, when an abnormal region in liver has a shape like a right lung, as shown for illustrative purposes in Figure 4. In such scenarios, contextual information helps resolve the ambiguity and redundancy examinations across different scales.

Figure 4

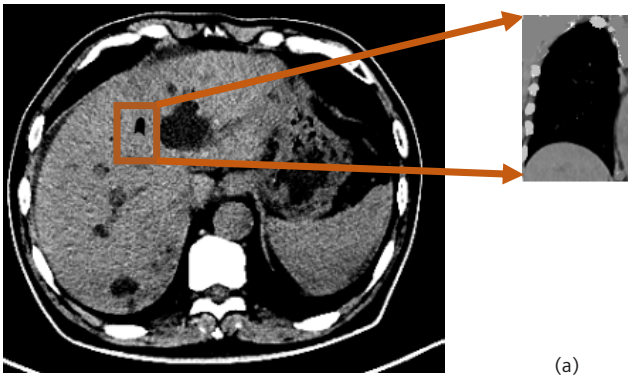

(a)

(b)

Figure 4. Liver image with artificially inserted abnormality for illustration purpose, and the zoom of the inserted defect (a), and coronal thoracic view (b). On a coarse scale, the artificially inserted region looks like just another abnormal region in the liver, however, a finer scale shape of the same region appears similar to the right lung region and traditional algorithms may detect candidate lungs landmarks (eg, apex of right lung) in this region. However, such a discrepency can be detected and ruled out by the ALPHA through the voting mechanism.

3. Redundancy via voting on other anatomical landmarks

Due to redundancy design during the detection, multiple candidate anatomical landmarks are detected independently. In this step, every landmark casts a vote for every landmark. Thus, each detected landmark serves as a candidate and a voter. Voting exploits redundancy of spatial relationships between landmarks in a way where correct landmarks reinforce each other, and incorrect landmarks are voted out. The cumulative information is used to define landmark locations with both confidence, and precision. The illustrative example in Figure 5 demonstrates how ALPHA landmarking achieves robustness through redundancy. This example shows four candidate landmarks for the "Right Costodiaphragmatic Recess," which have similar image features. Correct landmarks are positively reinforced by being voted in (thick lines), while incorrect landmarks are voted out (thin lines). Both local and distant anatomy is accounted for during the voting.

The algorithm accuracy is based on the following: performance evaluations using at least 200 clinically relevant cases, all landmarks are correctly detected, at least 85% of the cases with no more than 5% of false positives. With the reference hardware[a], the execution time for detecting landmarks is not more than one second per landmark on average.

Figure 5

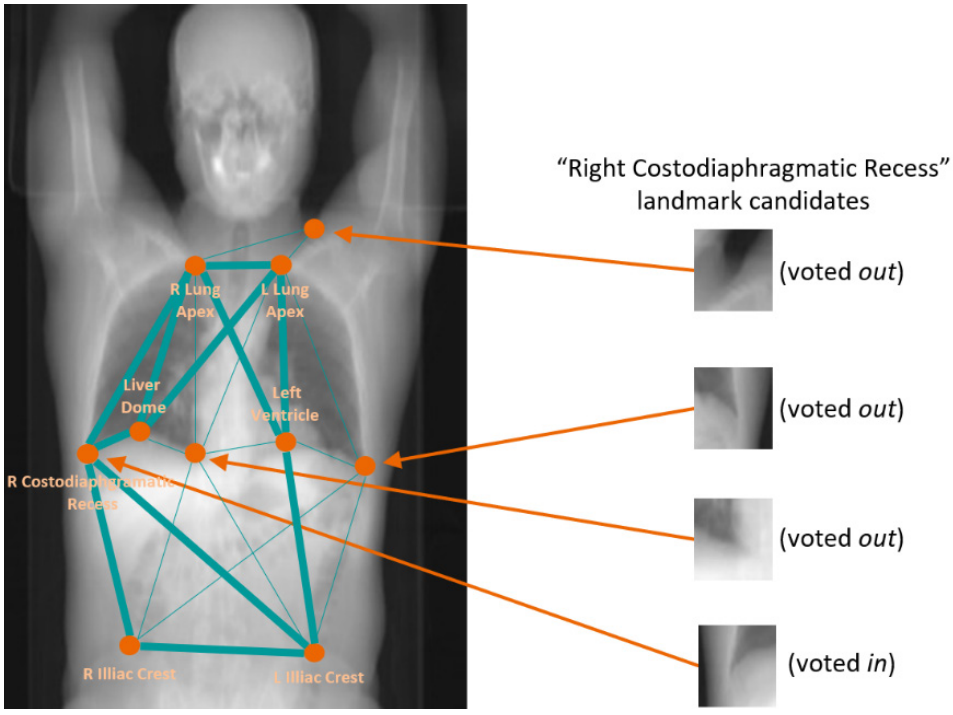

Figure 5. Illustrative example demonstrating the voting mechanism of ALPHA landmarking algorithm

[a] CPU: 4 cores, 64 bit; RAM:>=32 GB

Applications on intelligent PET/CT scanner platform (AIDAN)

The intelligent imaging platform, AIDAN, for our Biograph™ family of PET/CT scanners, includes the proprietary ALPHA technology to bring artificial intelligence to PET scanner operations, enabling more efficient, personalized, and standardize exams. The four features enabled by the AIDAN platform[b] are shown in Figure 6.

Figure 6

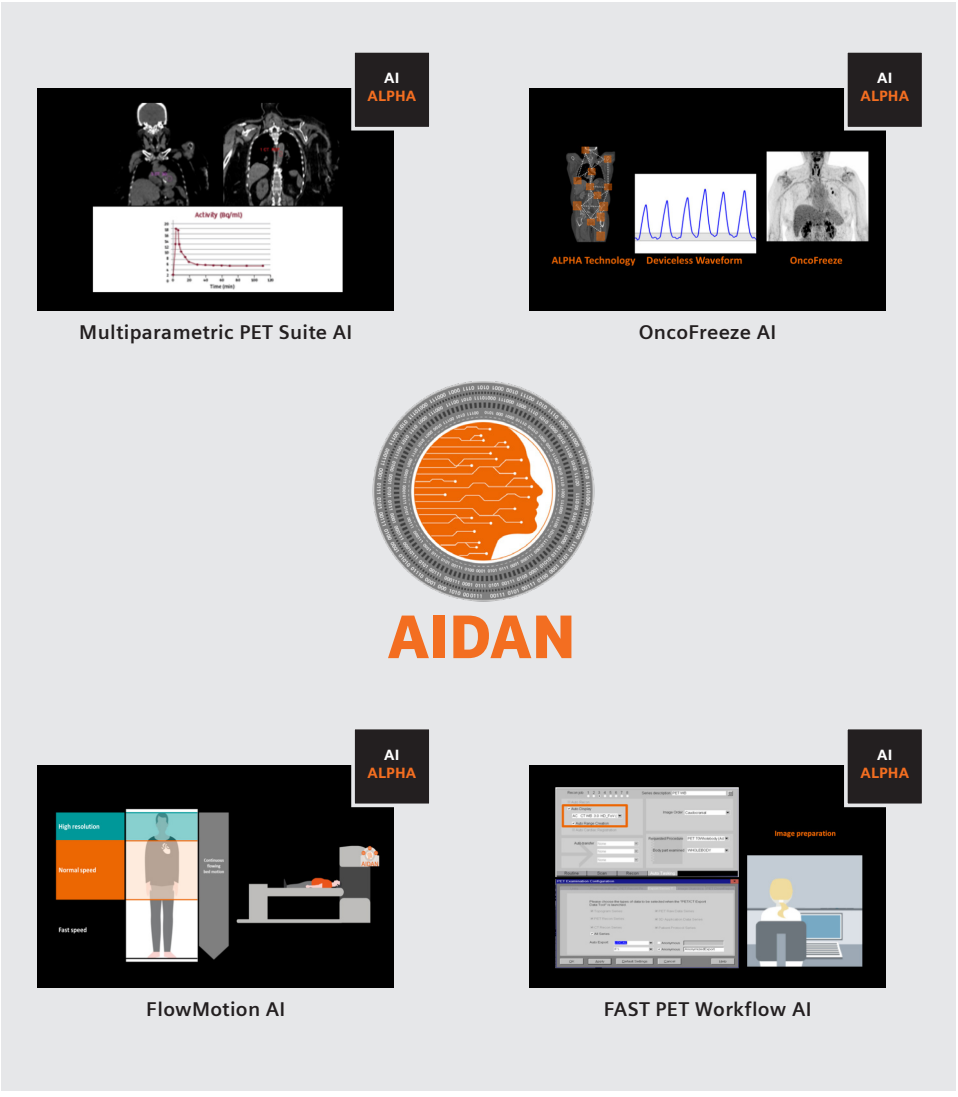

Figure 6. ALPHA-powered scanner features in the AIDAN platform.

[b] AIDAN platform scanner software version VG80/VJ30

FlowMotion AI

FlowMotion AI integrates FlowMotion[8] continuous bed motion technology and anatomical algorithms to automatically plan scan ranges using a CT topogram. With FlowMotion AI[9], landmarks associated with the top of the head, beneath the eye orbits, the clavicle, the aortic arch, the adrenal gland, the mid-thigh, and the tip of the toes are obtained from the CT topogram and used to establish PET scan ranges routinely used within clinical workflows. Figure 7 and Figure 8 illustrate the *PartialBody* and *TotalBody* configurations, respectively, which are typically defined on anterior-posterior (AP) topograms. The *PartialBody* options represent "eyes-to-thighs" scans, with optional lung and head-neck ranges. The *TotalBody* options span from the top of the head to the tip of the toes, and include configurations for lung, head-neck, and legs ranges. Additionally, an AP heart and a lateral brain range are also offered for single bed acquisitions, as shown in Figure 9. The heart and brain ranges are designed to respectively position the heart and cerebrum in the center of the field of view (FoV).

Figure 7

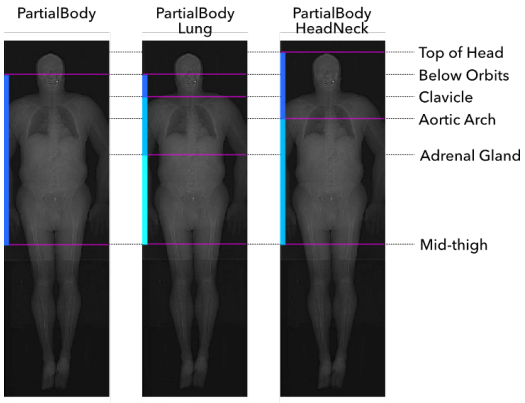

Figure 7. *PartialBody* scan configurations in FlowMotion AI.

Figure 8

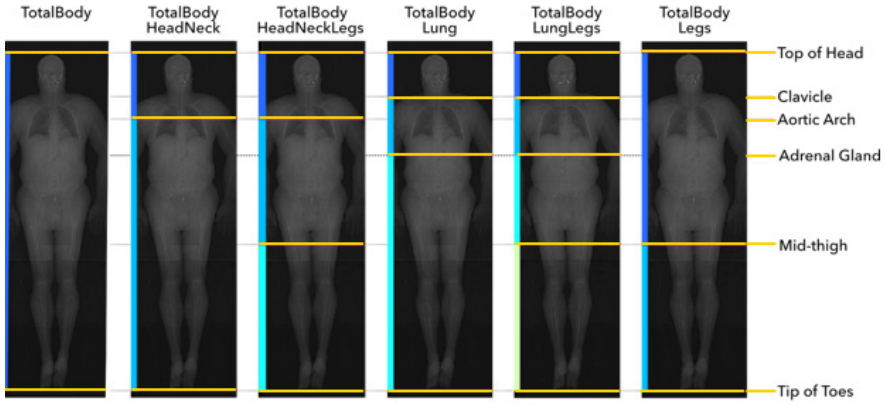

Figure 8. *TotalBody* scan configurations in FlowMotion AI.

Figure 9

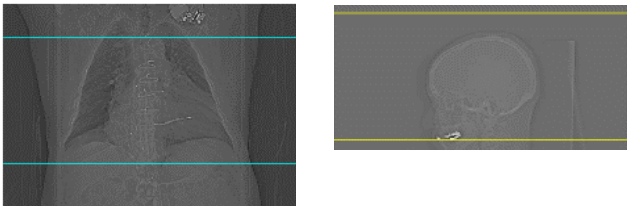

Heart Brain

Figure 9. Heart (a) and brain (b) scan configurations

FlowMotion AI enables a PET acquisition that can be personalized for an individual patient but standardized in clinical protocol strategy. This is achieved by specifying one or more scan ranges, as is exemplified in Figure 10, and setting corresponding bed speeds for each range. For example, Figure 10c illustrates a protocol strategy customized for colorectal or prostate cancer, where the speed is reduced within the pelvic and abdominal region to improve image statistics in the most clinically relevant area. The bed speed can also be increased substantially outside the boundary of the region of interest (ROI) to improve efficiency. Furthermore, respiratory gating strategies can be employed to a certain range to reduce the impact of patient motion.

Protocols can be stored, including the indication-based scan and reconstruction parameters according to hospital preference. This protocol can be reloaded to ensure reproducibility in multi-timepoint or follow-up studies and reduces user dependency.

Figure 10

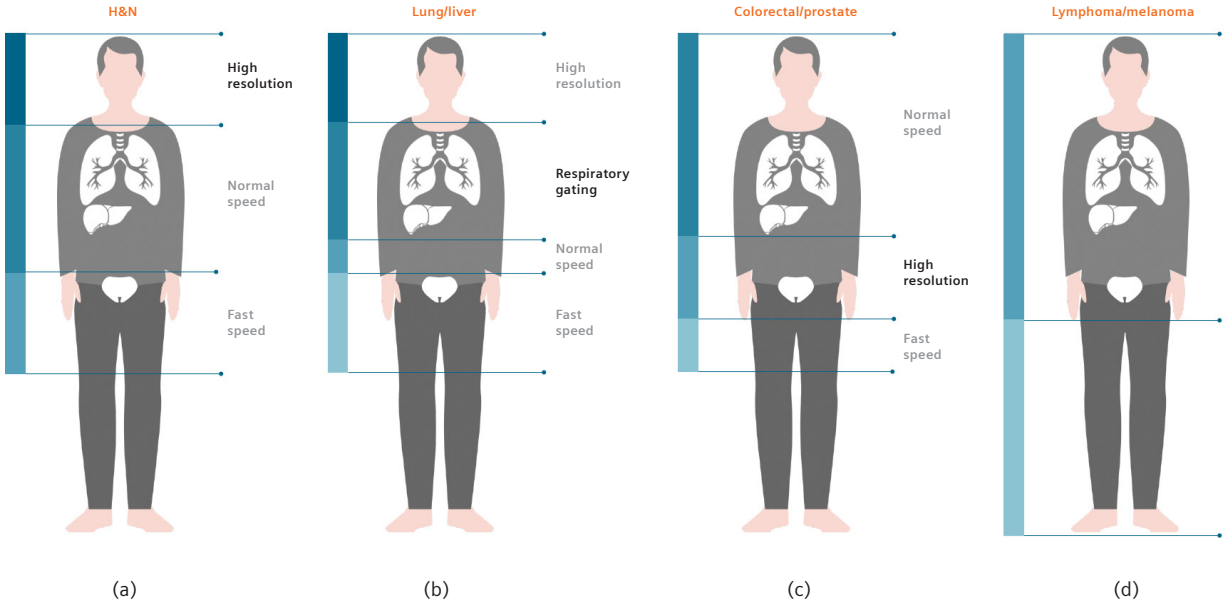

Figure 10. FlowMotion scan ranges can be tailored to patient anatomy and the clinical indication.

OncoFreeze AI

Physiological motion of internal organs causes motion-related blurring that affects quantification and delineation of the smallest detectable lesions and structures more severely, making compensation of respiratory motion in PET and PET/CT increasingly important.[10] Almost 90% of all oncological PET/CT cases involve lesions in the chest or abdomen.[10] In oncology, motion-related blurring is commonly seen in lung nodules and tumors, as well as in liver and pancreatic tumors.[11] Research shows that displacement happens in organs and lesions by a range of 5-30 mm, blurring images and reducing diagnostic confidence.[12] Without respiratory gating, 40% of lung lesions may even not be detected.[13] Thoracic lesions tend to be more susceptible to respiratory motion that can cause errors in definition of target volumes during planning of radiation therapy. However, image acquisition for PET requires several minutes, so lesion blurring due to respiratory motion is common. This can lead to an over-estimation of lesion volume, as well as under-estimation of radionuclide uptake by the lesion. However, challenges in respiratory motion management limit the use of gated images:

- Traditional motion management using physiological devices is labor intense and error prone to provide for every patient
- Setup of external physiological devices can add complexity and additional time to patient exams
- Acquiring enough counts to create a motion-frozen image often requires additional time to scan a patient if traditional gating approaches are being used

Figure 11

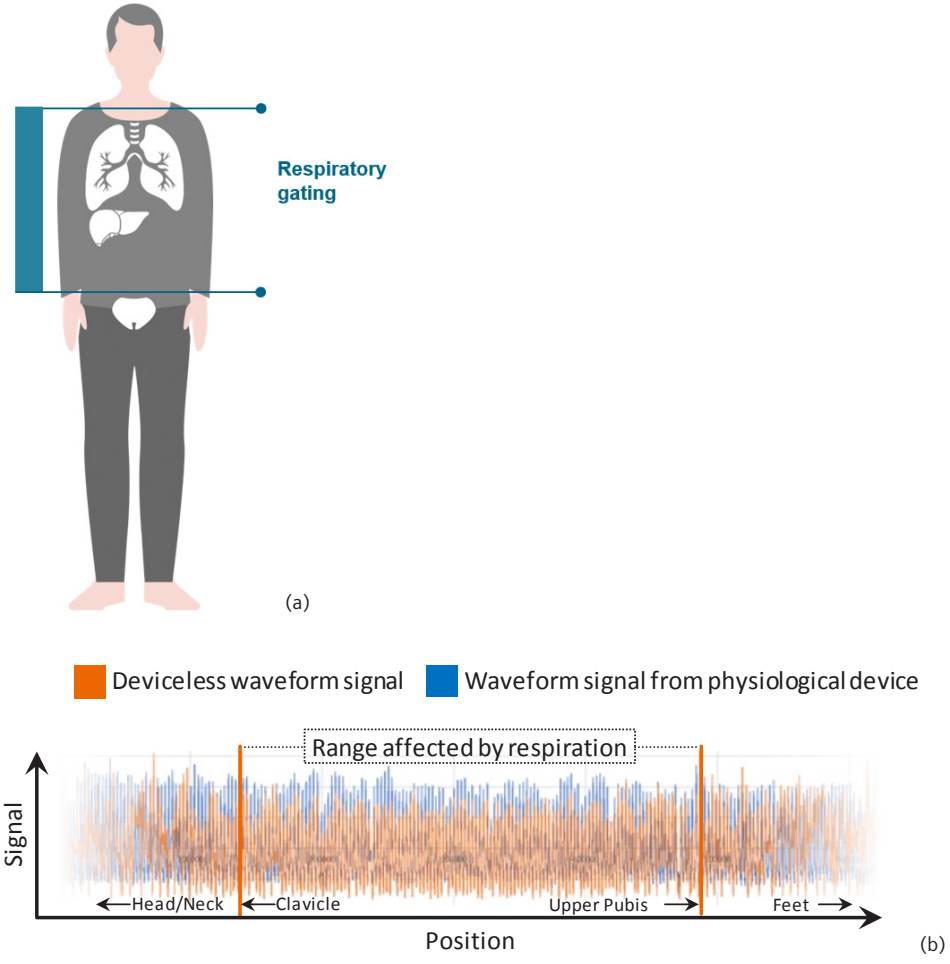

Figure 11. Shows the range of body to perform respiratory gating (a) and range of body habitus potentially affected by respiratory motion (b).

Siemens Healthineers OncoFreeze,[14-17] the existing solution for respiratory motion correction for oncology, consists of three distinct steps:

1. *Respiratory gating:* This step involves sorting of the acquired raw data into different gates based on the point in the respiratory cycle, at which the events were detected

2. *Estimation of Motion Information:* In this step images reconstructed from the gated raw data are used to estimate motion between the gates

3. *Motion Correction:* Information from previous two steps is then applied to the image reconstruction to generate motion-corrected PET images

OncoFreeze AI benefits from its predecessor, OncoFreeze.[14-17] Both solutions support the generation of motion-frozen images without any additional scan time; however OncoFreeze AI does not require an external gating device.

OncoFreeze AI is designed to offer motion-frozen PET images in areas affected by respiratory motion (as shown in Figure 11) by enabling a simple check box on the scanner UI. This feature for oncological whole-body acquisitions enables deviceless respiratory motion correction by integrating the Siemens Healthineers deviceless waveform technology and eliminating the need for external respiratory sensors. With FlowMotion[1] as the foundation for image acquisition, the scanner bed moves continuously. ALPHA technology identifies anatomy that typically is impacted by

Figure 13

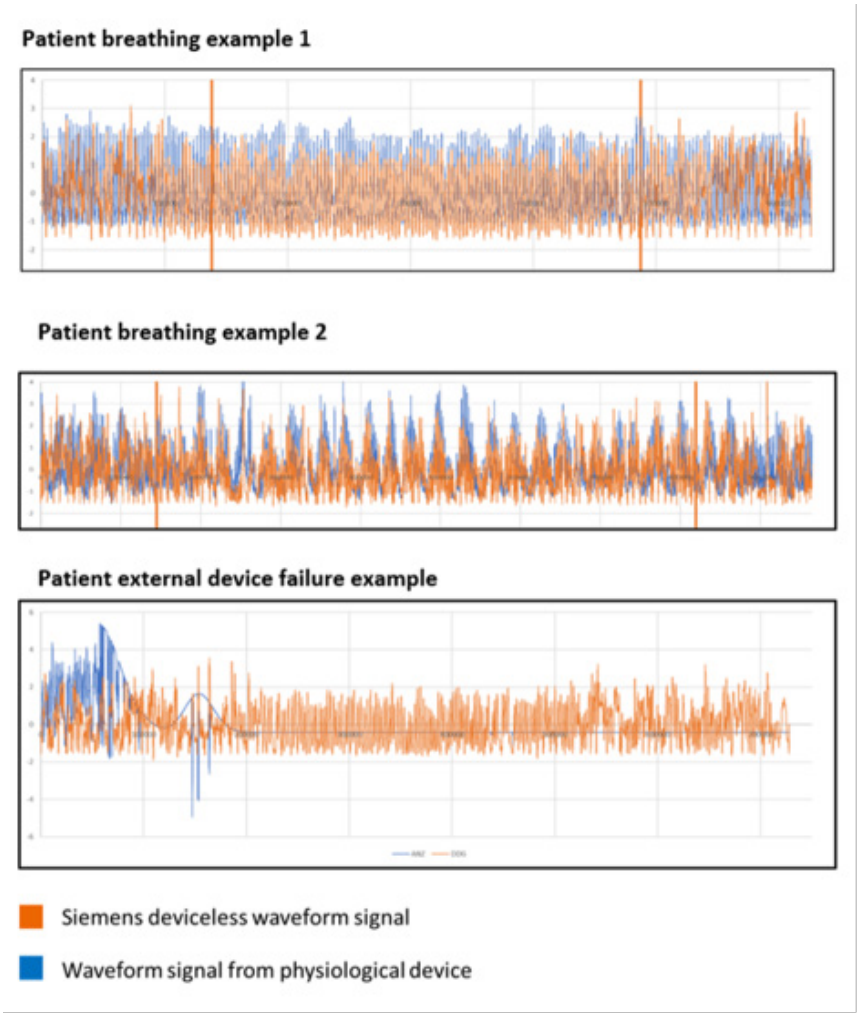

Figure 13. Sample Siemens Healthineers deviceless waveform signal.

respiratory motion, and the deviceless waveform technique generates the respiratory signal without any additional setup or patient interaction. Representative waveforms from three patients are shown in Figure 13. Finally, using OncoFreeze[14-17] for the image reconstruction, 100% of the acquired PET counts can be used for image reconstruction, which means no additional scan time for a motion-frozen image. An example image comparison between static and OncoFreeze image is shown in Figure 14.

OncoFreeze AI, being a deviceless approach for motion correction, also improves patient experience by eliminating the need of external device and helps to acquire high-quality images with no additional scan time.

Figure 14

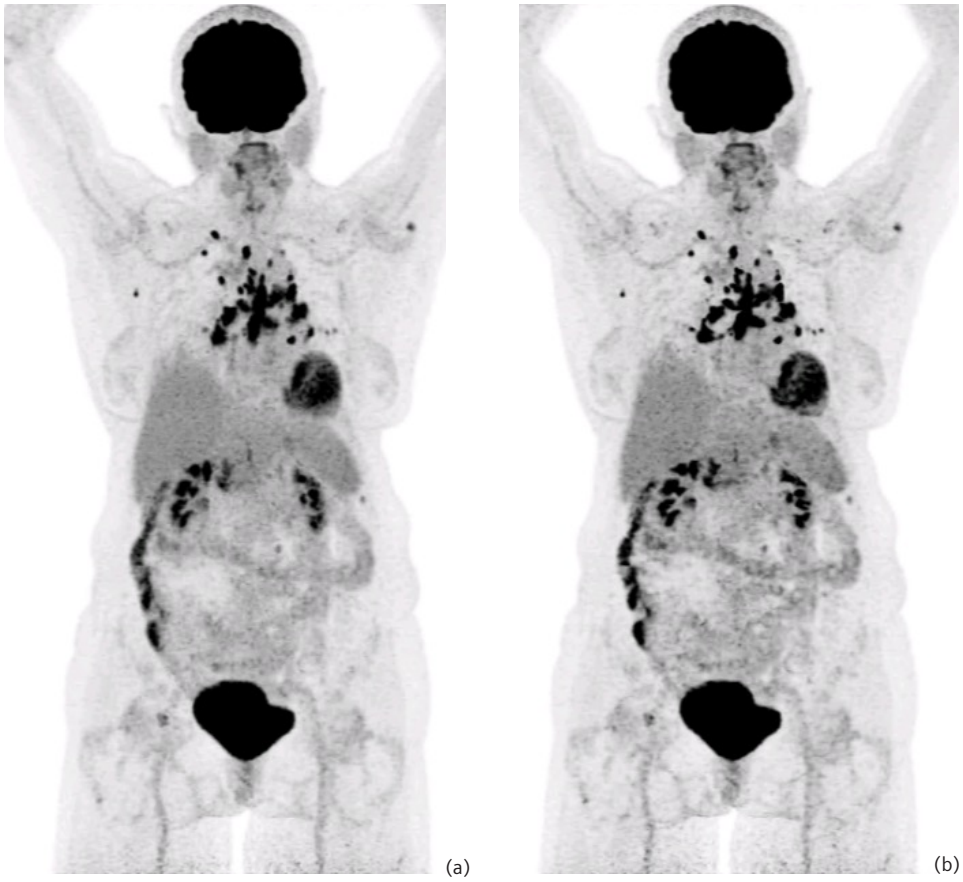

Figure 14. Comparison of static MIP and OncoFreeze MIP. Data courtesy of University Medical Center Groningen, Groningen, The Netherlands. Injected dose: 5.1 mCi (190 MBq), ^{18}F-FDG; Scan acquisition: 440 x 440 matrix, PSF + TOF 4i5s, 0.8 mm/sec FlowMotion continuous bed motion.

Multiparametric PET AI

The implementation of SUV facilitates the utilization of semi-quantitative metrics in the clinic for PET imaging. However, SUV cannot account for the PET tracer distribution over time—a dynamic process altered by several factors specific to each organ and ROI. Parametric analysis of dynamic PET helps to measure in vivo physiological processes such as ^{18}F fluorodeoxyglucose (^{18}F FDG) metabolism (MRFDG), blood perfusion, oxygen consumption, cell proliferation, and receptor density. MRFDG can be used to infer the glucose metabolic rate (MRGlu) with corrections for metabolic differences between ^{18}F FDG and glucose, but, due to a typically cumbersome workflow to perform MRFDG, its measurement remains a large, unmet need in the clinic to both stage and monitor cancer treatments.[18]

The intense manual effort for measuring MRFDG obtained based on Patlak modeling[18] is no longer required with the implementation of Multiparametric PET Suite AI, which leverages several unique innovations to provide a robust solution: FlowMotion continuous bed motion technology, whole-body (WB) dynamic imaging, ALPHA technology, and direct reconstruction (see Figure 15).

Figure 15

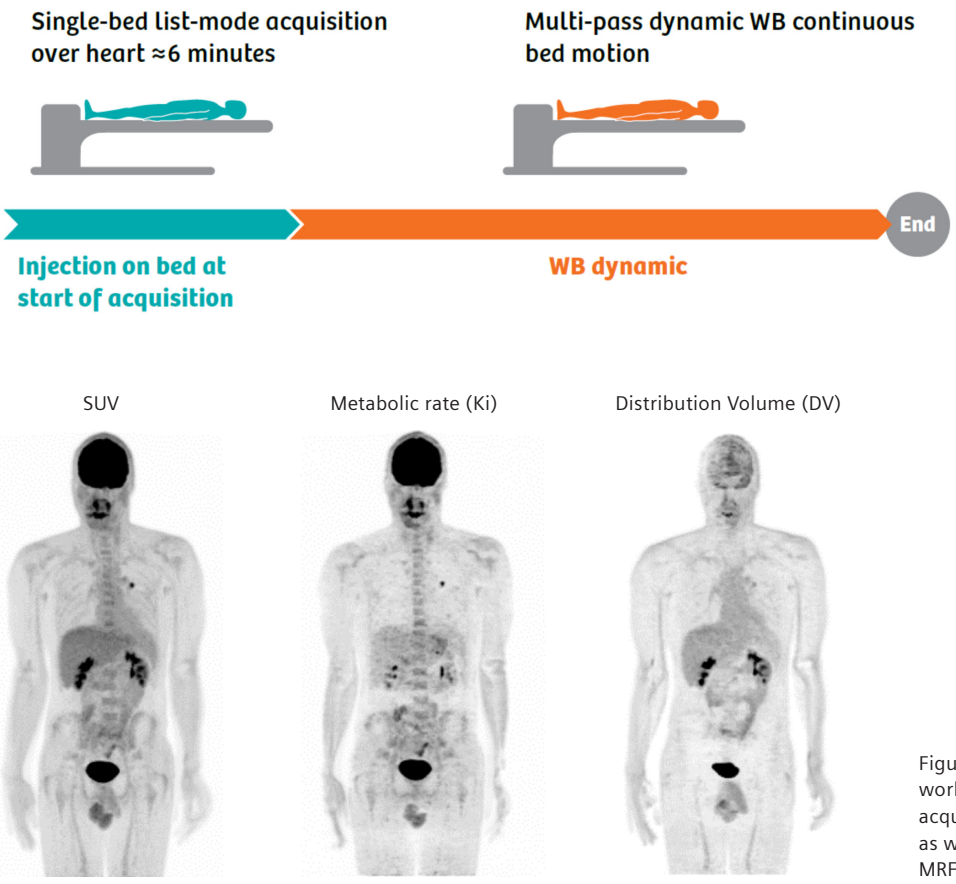

Figure 15. Multiparametric workflow showing FlowMotion acquisition (a) and SUV as well as derived images—MRFDG and DV (b).

The Patlak model is a graphical analysis technique based on a compartment model to estimate the dynamic physiological process of PET using linear regression.[18] The acquisition protocol for parametric PET differs from the standard SUV acquisition protocol. The subject is either injected on the bed at the same time as the PET acquisition is started (Figure 15), or the initial bolus concentration in the blood is estimated using non-imaging techniques. The input function obtained via non-imaging techniques, such as blood draws, can be invasive and requires significant manual intervention, prohibiting its use for routine clinical practice. Research has shown that an image derived input function can be substituted for invasive blood draw techniques.[18-19] However, a user is required to manually draw the ROI in a blood pool region, eg, descending aorta or left ventricle, which can be automated with the use of AI technology.

In this fully automated approach, CT and dynamic PET data are used to generate an image-derived input function (IDIF). Using ALPHA technology, landmarks are found in left ventricle (LV) and proximal descending aorta on the CT images. The CT reconstruction that is used for the PET attenuation correction (AC_CT by default) is used to find these landmarks. These landmarks are transferred to the PET image to create the volume of interest (VOI) around the landmark point in the descending aorta (cylinder: 5 mm radius, 20 mm height), and LV (30 mm diameter sphere). The IDIF can therefore be automatically generated from both the LV blood pool and proximal descending aorta using ALPHA as shown in Figure 16.

An internal analysis on 110 WB AC_CTs showed a success rate of >95%. Potential reasons for failure are incomplete CT scan coverage over the heart and descending aorta regions, or if the algorithm reports low confidence in the location of the landmark. If an input function VOI is not found automatically, the user will be required to generate one manually on the scanner console, export the time activity curve, and reload it into the scanner user interface.

Figure 16

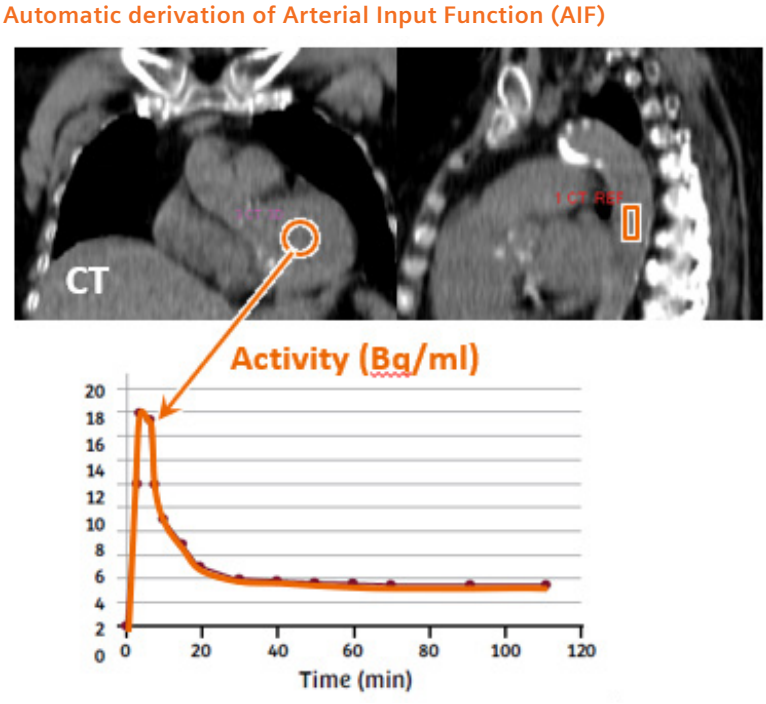

Figure 16. Image derived input function from left ventricle and placement of reference region in the aorta.

AI algorithm identifies anatomical landmarks.[1]
Region of interest (ROI) is defined, eg, descending aorta.
AIF is derived using dynamic images and ROI.

FAST PET Workflow AI

Once the scan is complete, technologists may still have multiple tasks on the scanner console to prepare a patient exam for reading and archiving. Such additional tasks limit time for a technologist to spend on patient care. Additionally, such repetitive tasks that could be automated can influence reduction of technologist fatigue.

Radiologists have no need to review blank images (as shown in Figure 17; depicted by red lines), as it is inefficient to manually scroll through air as well as taxing on the data storage systems. Technologists therefore often manually review images and either define ranges to remove blank images or auto-create ranges and subsequently select the images containing tissue to be sent to picture archiving and communication system (PACS).

Fully Assisting Scanner Technologies (FAST) Workflow Auto PACS-ready ranges use ALPHA to identify a skin-to-skin range of images and automatically creates ranges with anatomy present in the images. Figure 17 illustrates an example with the eliminated slices in red and useful slices shown in white. With the FAST PET Workflow AI feature, we remove the blank images in coronal, sagittal, and axial views. Additionally, images can be exported to a predefined storage location at any specific time of the day. Since blank slices are removed, it also helps to reduce the storage space for PACS, as shown in Figure 18.

Figure 17

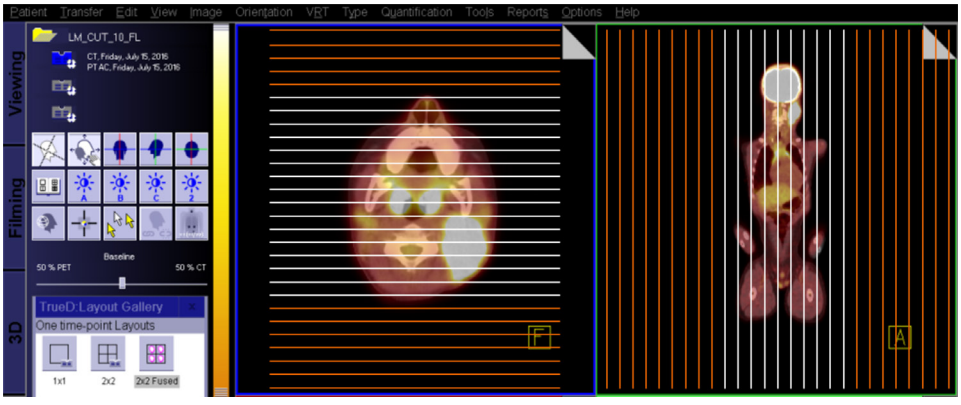

Figure 17. Eliminated slices are shown in red and retained slices encompassing the anatomy are shown in white.

Figure 18

	#of images: traditional			#of images: fast			#of blank images removed
	CT	PET	Fused	CT	PET	Fused	
Transaxial	325	325	325	324	324	324	3
Sagittal	155	145	155	127	127	127	74
Coronal	155	145	155	70	70	70	245

- **Without blank image removal these images would have to be deleted from the patient browser manually before being exported.**
  - **This results in 54 additional user interactions per patient examination.**
  - **Also conserves system storage space. In one example 0.51 GB less than orginal.**

Figure 18. Sample reduction in blank slices and storage space.

MI applications on the *syngo*.via intelligent reading solution

AI-powered applications in *syngo*.via to enable efficient clinical analysis of PET and SPECT images are shown in Figure 19.

Figure 19

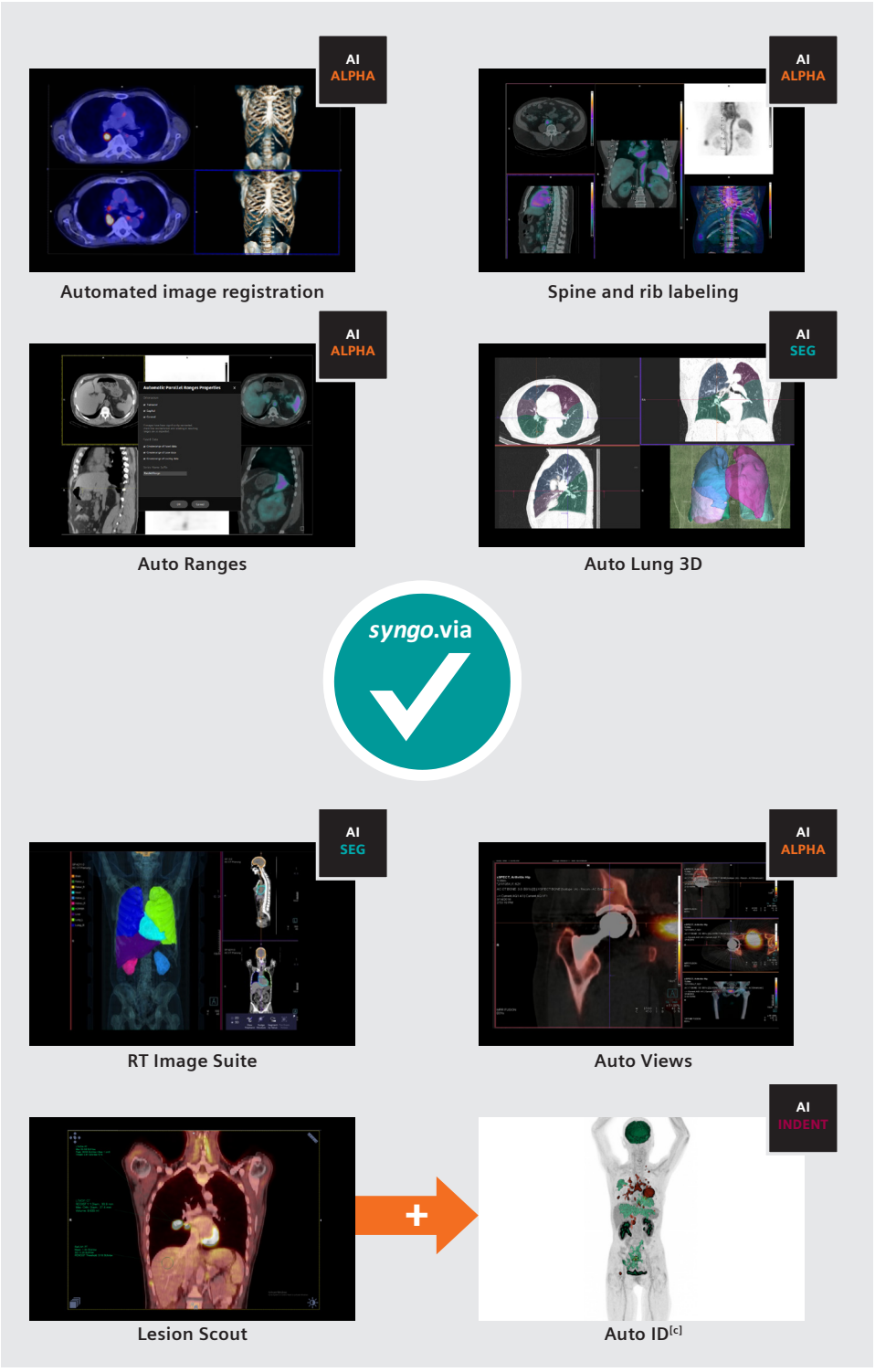

Figure 19. MI *syngo*.via applications incorporating ALPHA technology.

[c] Lesion Scout with Auto ID is not available for sale in the USA and is not commercially available in all countries. Future availability cannot be guaranteed. Please contact your local Siemens Healthineers organization for further details.

Automated image registration

The utility of molecular imaging is expanding in the selection of patients who would most benefit from targeted therapy, early treatment responders to predict therapeutic efficacy, and tumor response to survival.[20] Clinicians need to visually compare the same lesion(s) from two or more timepoints but also quantitatively measure SUV changes.

Traditional image registration algorithms have helped clinicians by automatically spatially aligning studies from multiple timepoints. These conventional algorithms often have limitations when imaging conditions change from one timepoint to the other, for example, with different FoVs (see Figure 20), or with patient posture changes (eg, hands-up versus hands down), or with different patient table setup (eg, a thick versus a thin cushion). Traditional image registration algorithms using pixel-by-pixel comparison logic may find a "local minimum" by, for example, matching shoulder with pelvis or by matching up the two tables instead of the patient anatomy. Clinicians must perform manual alignment of the image volumes if the algorithm fails. This is a tedious task which reduces throughput and can cause reader fatigue when reading many cases.

As described previously, ALPHA can automatically recognize anatomical structures in medical images and is well suited to the task of robust image registration. Depending on the anatomical scan range, ALPHA detects multiple (> 4) landmarks in each study, filters them based on an anatomical consistency check and uses the overlapping landmarks to align studies from different time-points. Because ALPHA registration is based on recognition of anatomical structures just like the way a human observer would do it, instead of low-level pixel matching, it is robust to the variations mentioned above. Figure 21 shows an example with grossly mismatched CT FoVs, where ALPHA landmark-based registration is still robust for lesion tracking.

Furthermore, as ALPHA's capability is learned from examples and trained to recognize landmarks in MRI images as well, it can even align studies from different modalities (CT/MRI) as shown in Figure 22.

Figure 20

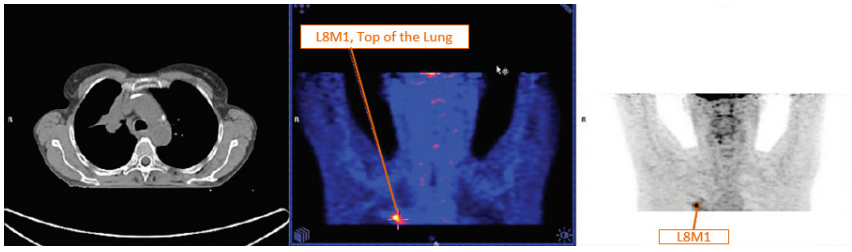

(a)

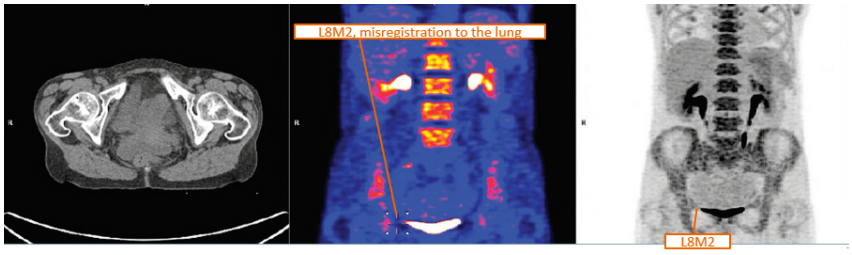

(b)

Figure 20. Registration of two studies with different FoVs—Head&Neck region and extended torso region with no common overlap region. Baseline image shown to have lesion (L8M1) in Head&Neck region (a). Follow up scan shown in (b), where registration of baseline and follow up performed using "optimal" pixel-based match registration algorithm resulted in matching the lesion (L8M1) at top of the lung with area in pelvis region (L8M2) on follow-up scan. While tracking lesions over time, a reader will have to correct for misregistration to look at trends for a particular lesion over time.

Figure 21

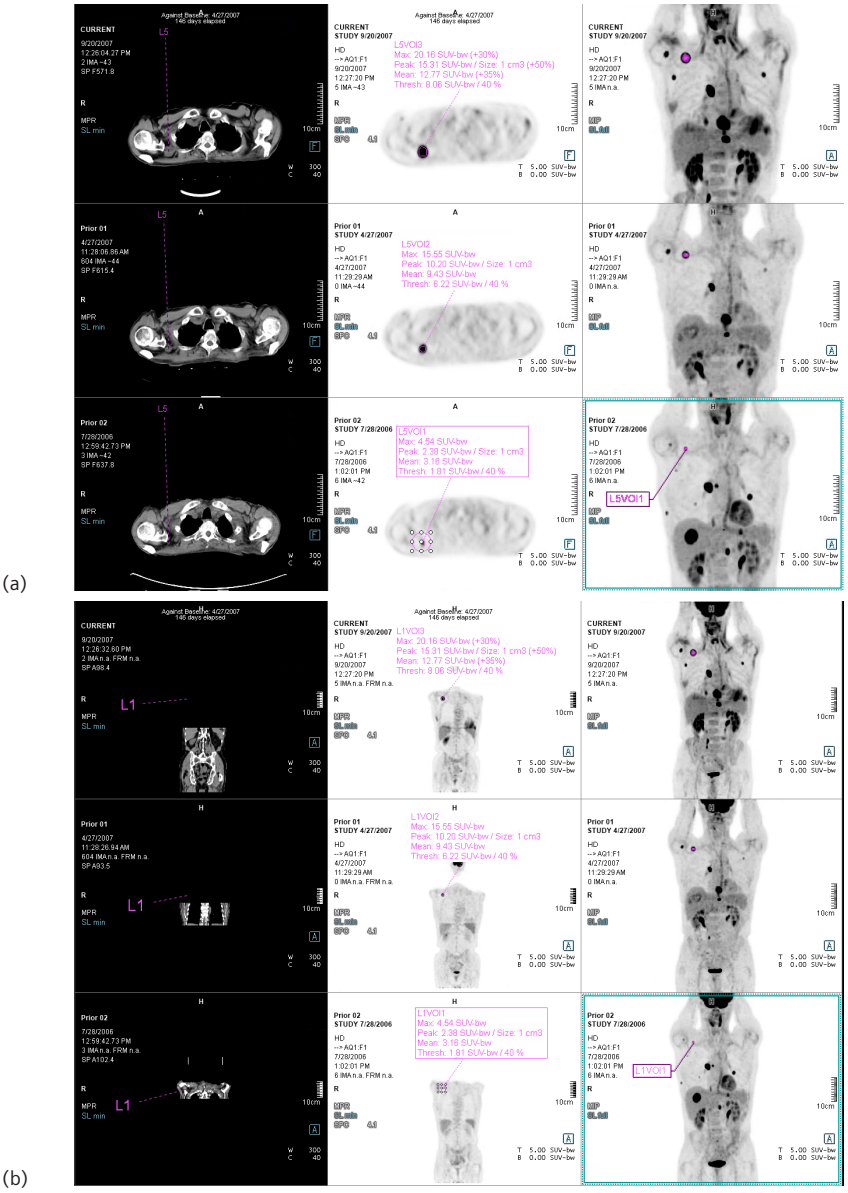

Figure 21. Alignment of multiple time-point studies using ALPHA registration full length CT available at all time point (a) and non-overlapping region (b).

(a) The lesion on Prior2 L5VOI1 (bottom row) is automatically registered to the same lesion on follow-up scans L5VOI2 (Prior1, middle row) and L5VOI3 (current, top row) when full images CT images are available for registration.

(b) To demonstrate the robustness of registration algorithm based on ALPHA-landmarks, a new dataset was created so that CT images on all three timepoints from (a) had different FoVs. These timepoints were again loaded in syngo.via MM Oncology to see if registration (performed with on CT images) was robust for tracking the lesions. The PET FoV was not changed. The lesion on Prior2 L1VOI1 (bottom row) is automatically correctly registered to lesion on follow-up scans L1VOI2 (prior1, middle row) and L1VOI3 (current, top row) even when CT images do not have matching FoVs. While performing ALPHA-landmarking the algorithm can predict the location of landmarks that are not present in the FoV, which enables a very robust registration.

Figure 22

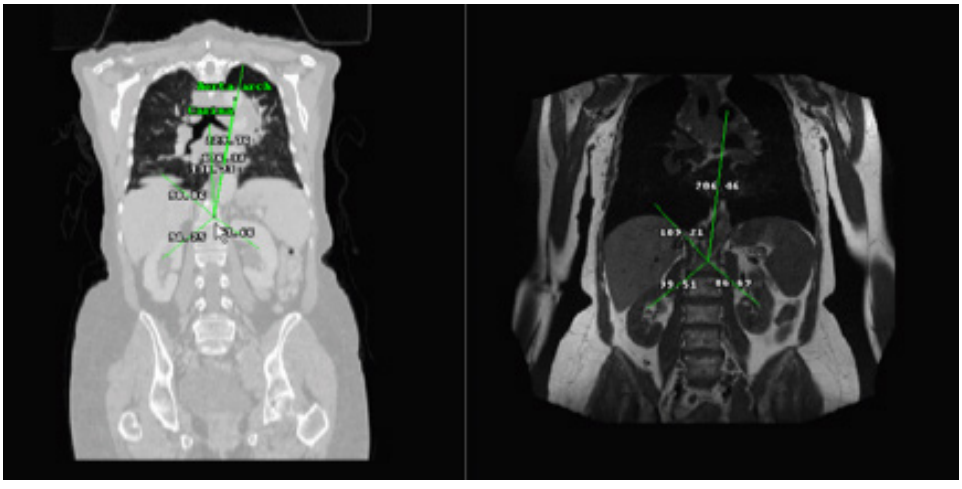

Figure 22. Multi-modality registration between CT image (a) and MRI images (b). Various landmark points are common between MRI and CT images. Registration algorithm is optimized to register those landmark points between two images to get the optimal alignment. Registration is robust even when the CT image is acquired with hands-up, while the MRI image is acquired with hands down.

Creation of reference regions for Lesion Scout and Deauville criteria

Lesion Scout (formerly known as Multi-Foci Segmentation (MFS) in previous versions of *syngo*.via) is designed to offer the reading physician a way to segment uptake and create findings based on pre-selected criteria. Lesion Scout works on PET or SPECT data from any quantitative reconstruction that results in data with SUV values and is agnostic of the tracer used. This enables the reader to customize the segmentation criteria to varying clinical needs, different radiopharmaceuticals, or local site segmentation preferences. This feature may also aid in removing inter-user variability because the parameters used for segmentations can be easily and repeatably applied by different reading physicians, supporting manual as well as PERCIST-based measurements.[21]

PERCIST recommends the use of reference ROIs positioned either in the right lobe of the liver or the descending aorta, to determine reportable lesions or to quantify changes in lesion uptake across timepoints. To manually draw and place an ROI of a particular size in a consistent and appropriate location inside the liver or descending aorta is not a difficult task for the clinician, but surely a tedious one, especially if PERCIST criteria is used on all the patients.

ALPHA landmarking supports the automatic placement of reference ROIs in the liver and in the descending aorta using the CT image. ALPHA detects multiple landmarks in and around the liver and the descending aorta and uses all of them to infer and confirm the final placement of the two ROIs. As a result, the reference ROI detectors are very reliable despite changes in image contrast and highly robust to abnormalities such as calcifications in the aorta or lesions in the liver. The landmarks are transferred to PET image and ROIs are centered around these (see Figure 23).

Figure 23

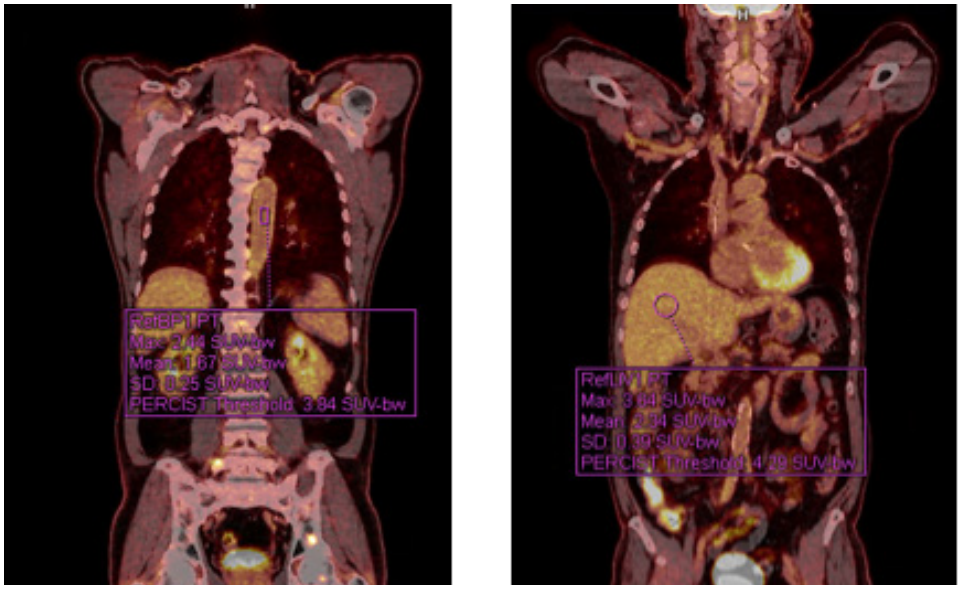

(a) (b)

Figure 23. Reference region identified by ALPHA to calculate the PERCIST threshold in blood pool (a) and liver (b).

Deauville criteria

The Deauville scale is an internationally recommended scale used by physicians in staging and assessment of treatment response in Hodgkin lymphoma (HL) and certain types of non-Hodgkin lymphomas (NHL).[23] This criterion provides a simple visual assessment of FDG uptake in the hottest lesion relative to blood and liver reference regions.

A Deauville score is calculated for each lesion as shown in Figure 23, and the score for the hottest lesion can be assessed across timepoints in the trending tab, as shown in Figure 24. The Deauville criteria[21] are evaluated on a scale from 1 to 5, where 1 is the best and 5 is the worst:

1 - No uptake
2 - Uptake ≤ mediastinum
3 - Uptake > mediastinum but ≤ liver
4 - Moderately increased uptake compared to liver
5 - Markedly increased uptake compared to liver and/or new lesions (Markedly increased uptake is taken to be uptake > 2-3 times the SUV_{max} in a normal liver.)

Figure 24

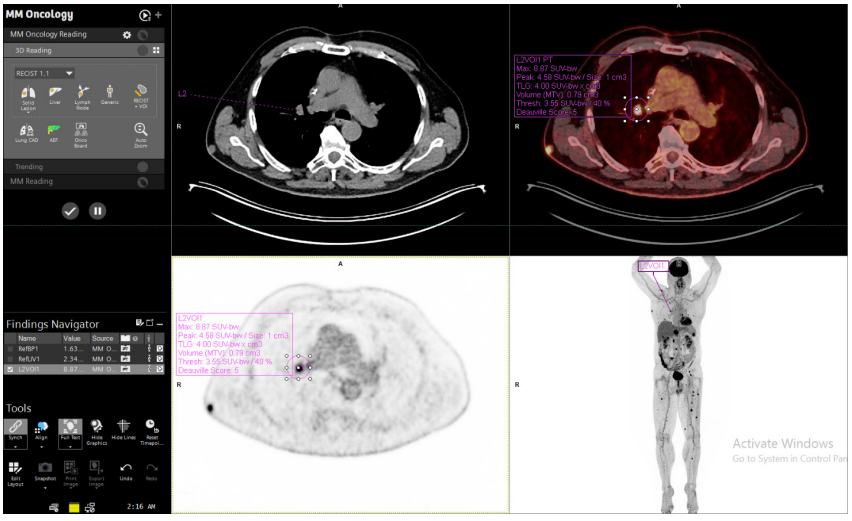

Figure 24. 24 Deauville score calculation for a segmented lesion.

Data courtesy of Le Centre Hospitalier Universitaire Vaudois (CHUV), Lausanne, Switzerland.

Figure 25

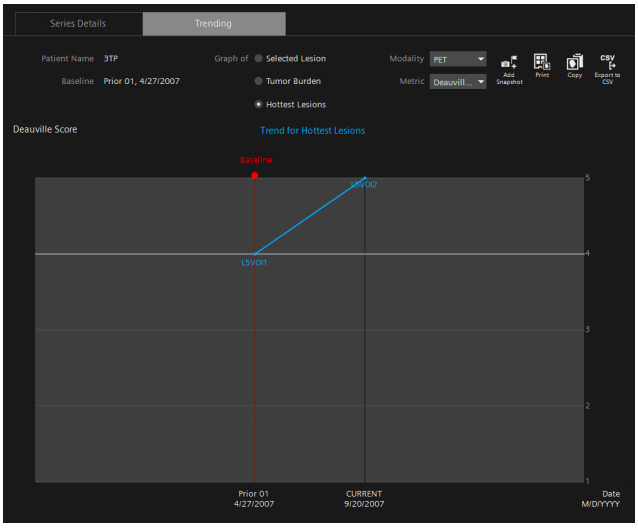

Figure 25. Trend of hottest lesion by Deauville score baseline has a score of 4, and, at the follow-up, the score is 5.

Spine and rib labeling

The spine consists of 33 vertebrae (7 cervical, 12 thoracic, 5 lumbar, 5 fused sacrum, 4 fused coccyx), 23 intervertebral disks, the spinal cord, and connecting 24 ribs, making it a complex anatomy. Hybrid technology (SPECT/CT or PET/CT) is a sensitive tool to detect skeletal metastasis in known malignancies. However, its high sensitivity and low specificity may account for false positive diagnosis in cases of trauma, infection, inflammation, and other benign conditions. When detecting such skeletal metastasis, careful review is required by a reading physician, necessitating accurate anatomical correlation with findings on hybrid imaging.[22 -25] For the spine and rib labelling, ALPHA detects the center of each vertebral body and suggests its label (C1-C7 in cervical, T1-T12 in thoracic region, L1-L5 lumbar region, S - sacrum) along with the ribs (right 1-12, left 1-12) in CT datasets, as shown in Figure 26.

Figure 26

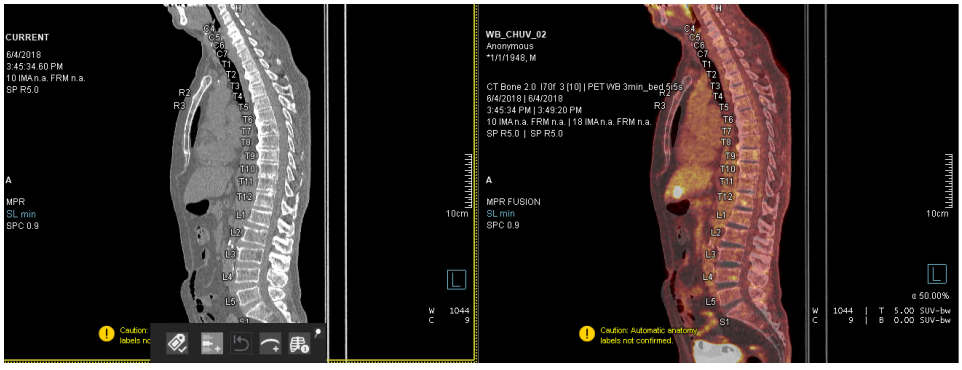

(a)

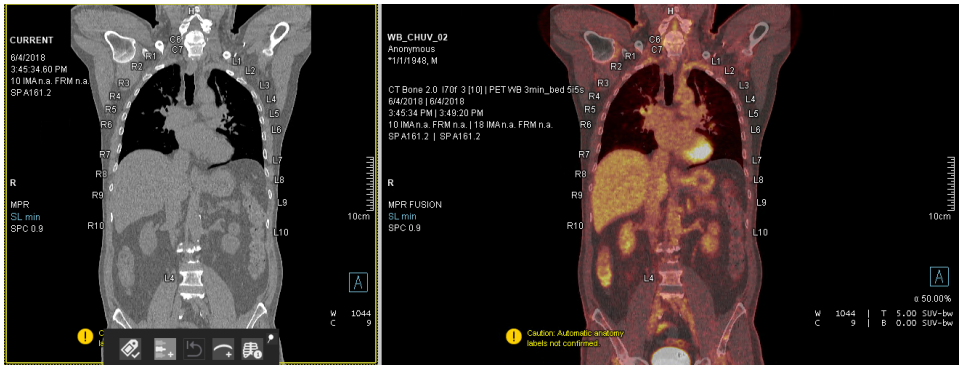

(b)

Figure 26. FDG PET/CT scan demonstrating overlay of vertebra labels (a) and rib labels in (b); label (C1-C7 in cervical, T1-T12 in thoracic region, L1-L5 Lumbar region, S - sacrum) and ribs (Right 1-12, left 1-12).

Data courtesy of
Le Centre Hospitalier Universitaire Vaudois (CHUV), Lausanne, Switzerland.

Auto views

Increasing use of molecular imaging in non-oncology applications, eg, orthopedics, requires re-orientation of CT and fused (PET/CT or SPECT/CT) datasets based on the anatomy of interest or when data is prepared for a report. It may be required, for example, to re-orient the patient anatomy to be the same as a baseline scan. Additionally, for each patient anatomy of interest is re-oriented in a consistent manner that can help to standardize the reading report. Auto Views functionality helps to eliminate manual steps to re-orient images and zoom in on a required region. An ALPHA gallery shows landmark points and body regions, along with the preview of how image will be reoriented based on the user selection (Figure 27 (a)). When a user makes a particular selection, the ALPHA landmarking algorithm runs to detect the landmark and then re-orients image, as shown with an example in Figure 27 (b).

Figure 27

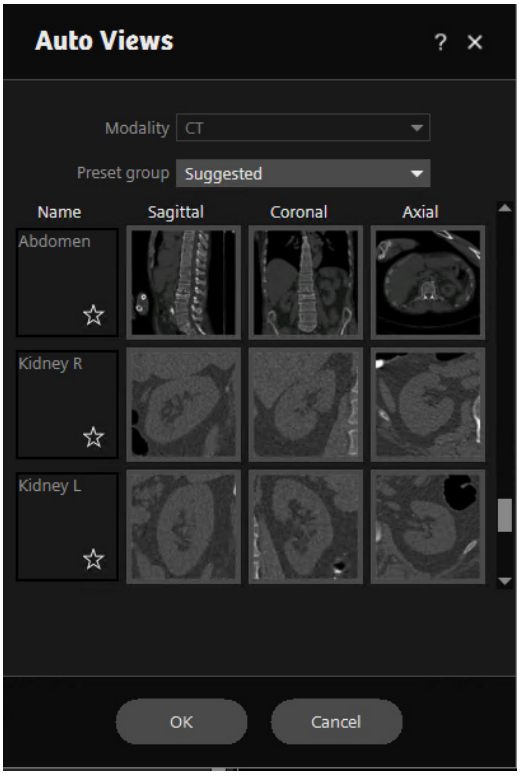

(a)

(b)

Figure 27. ALPHA gallery that shows three presets Abdomen, Kidney Right, and Kidney Left with a preview on how image will be re-orientated (a). Users can add any of the regions/ landmarks in a list of their favorites. Reorientation of hip region on xSPECT image using the Hip Acetabulum right anatomical landmark point (b).

Auto ranges

Radiologists have no need to review blank images, as described in the AIDAN platform feature *FAST PET Workflow AI*. However, images could come from non-Siemens Healthineers scanners, so this feature is also included in *syngo*.via. *Auto Ranges* uses ALPHA to detect the skin-to-skin images and creates ranges automatically only with anatomy present in the images, like the *FAST PET Workflow AI* feature on the PET/CT scanner. The newly created ranges can be transfer to PACS. Figure 28 shows the *syngo*.via application of creating parallel ranges that removes extra blank slices.

Figure 28

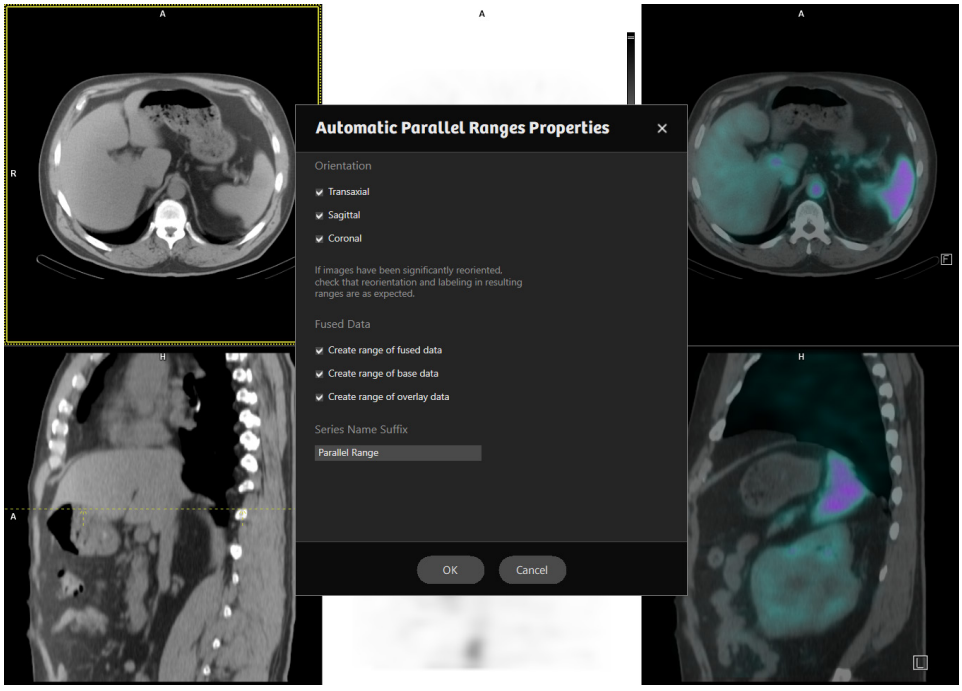

Figure 28. Parallel ranges created in syngo.via shows removal of unnecessary blank slices.

Conclusion

ALPHA technology reliably provides anatomical context and has been used to enrich applications on the AIDAN platform and *syngo*.via reading solutions. Scanner applications help to improve the patient experience by reducing the scan time and performing motion management without external devices. Automatic adjustment of scan parameters and multi-parametric analysis based on the anatomy and disease condition will open new opportunities for precision medicine. Applications in reading solutions enable optimal workflow solutions for performing daily clinical analysis, such as tracking lesion over time, placement of reference region for lesion segmentation or Deauville score measurement, and re-orienting images in standardize format for reporting purposes. Additionally, these applications are efficient to use, enabling reproducible and standardized results. Rather than performing mundane tasks in the workflow, results only need to be reviewed and verified before making any clinical conclusions. This will increase efficiency of both technologist and nuclear medicine readers and will allow them to focus on patients to improve patient experience and transform care delivery.

Acknowledgments

The author thanks Dr. Bruce Spottiswoode, Dr. Sven Zuehlsdorff, Dr. Anne Smith, Dr. Carl Von Gall, Dr. Gerardo Hermosillo Valadez, Dr. Zhigang Peng, Dr. Sebastian Fuerst, Ms. Jessie Reed, Ms. Katherina Swystun, Ms. Colleen Smith, and Ms. Nicole Trezciak for valuable discussions, contributions, and review of this document.

References

[1] **J. Czernin, I. Sonni, A. Razmaria, and J. Calais,** "The Future of Nuclear Medicine as an Independent Speciality," *JNM* 60(2):3S-12S, Sep 1 2019

[2] **P. Ghosh,** "xSPECT Bone: a clinical overview," White Paper, Siemens Healthineers, 2018

[3] **X. S. Zhou, Y. Zhan, Z. Peng, M. Dewan, B. Jian, A. Krishnan, M. Harder, R. Schwarz, L. Lauer, H. Meyer, S. Grosskopf, U. Feuerlein, and H. Ditt,** "Reliability and redundancy: reducing error cost in medical imaging", in: B Krishnapuram, S. Yu, and R. Rao (Eds.): Cost-Sensitive Machine Learning, Chapman and Hall/CRC, 2011

[4] **X. S. Zhou, Y. Zhan, V. C. Raykar, G. H. Valadez, L. Bogoni, Z. Peng, M. Dewan, M. Wolf, Y. Shinagawa, S. Park, M. Salganicoff, L. Raghupathi, and P. Devarakota,** "Mining anatomical, physiological and pathological information from medical images." SIGKDD Explorations 14(1):25-34, 2012

[5] **Y. Zhan, M. Dewan, M. Harder, A. Krishnan, X. S. Zhou,** "Robust automatic knee MR slice positioning through redundant and hierarchical anatomy detection," *IEEE Trans. Med. Imaging* 30(12): 2087-2100, 2011

[6] **Y. Tao, Z. Peng, A. Krishnan, X. S. Zhou,** "Robust learning-based parsing and annotation of medical radiographs." *IEEE Trans. Med. Imaging* 30(2): 338-350, 2011

[7] **W. Watanabe, A. Kitaoka, K. Sakamoto, M. Yasugi, and K. Tanaka,** "Illusory Motion Reproduced by Deep Neural Networks Trained for Prediction," *Front Psychol.* 15 March 2018 (https://doi.org/10.3389/fpsyg.2018.00345)

[8] "Technical and Clinical Advances with FlowMotion Technology," White paper, Siemens Healthcare GmbH, 2016.

[9] **D. Pigg and B. Spottiswoode,** "FlowMotion AI," White paper, Siemens Healthineers, 2019

[10] **P. J. Keall, G. S. Mageras, J. M. Balter, R. S. Emery, K. M. Forster, S. B. Jiang, J. M. Kapatoes, D. A. Low, J. M. Murphy, B. R. Murray, C. R. Ramsey, M. B. Van Herk, S. S. Vedam, J. W. Wong, E. Yorke** "The management of respiratory motion in radiation oncology report of AAPM Task Group 76." *Med Phys* 2006; 33:3874–3900

[11] BIO-TECH SYSTEMS, INC. Report 2008.

[12] **Grills, Inga S et al.** "Potential for reduced toxicity and dose escalation in the treatment of inoperable non–small-cell lung cancer: A comparison of intensity-modulated radiation therapy (IMRT), 3D conformal radiation, and elective nodal irradiation." *International Journal of Radiation Oncology, Biology, Physics,* Volume 57, Issue 3, 875-890.

[13] **Garcia Vicente AM, et al.** (18) F-FDG PET-CT respiratory gating in characterization of pulmonary lesions: approximation towards clinical indications. *Ann Nucl Med.* 2010 April 24 (3) 207-14

[14] **J. Hamill, P. Ghosh,** "HD Chest Respiratory Gating for PET," White Paper, Siemens Medical Solutions, USA, 2011

[15] **M. Dawood, F. Gigengack, X. Jiang, KP Schäfers,** "A mass conservation-based optical flow method for cardiac motion correction in 3D-PET." *Med Phys*. 2013;40:1-9.

[16] **I Hong, J Jones, M Casey,** "Ultrafast Elastic Motion Correction via Motion Deblurring." In; 2014 IEEE Nuclear Science Symposium and Medical Imaging Conference (NSS/MIC). IEEE; 2014:1-2

[17] **S Poesse, I Hong, D Mannweiler, et al.** "Respiratory motion compensation in PET/CT: Evaluation of a fast elastic motion compensation technique based on motion deblurring". *J Nucl Med* .2017;58(suppl 1):1349.

[18] **A. Smith, B. Spottiswoode, V. Shah, J. Hu, C. von Gall, "**FlowMotion Multiparametric PET Suite-The Patlak Model," White Paper, Siemens Medical Solutions USA, Inc. 2019.

[19] **D. Vriens, L. de Geus-Oei, W. Oyen, E. Visser,** "A Curve-Fitting Approach to Estimate the Arterial Plasma Input Function for the Assessment of Glucose Metabolic Rate and Response to Treatment," *JNM* 2009 Dec 50(12): 1933-9.

[20] **AR Pantel, DA Mankoff.** "Molecular imaging to guide systemic cancer therapy: Illustrative examples of PET imaging cancer biomarkers." Cancer Lett. 2017;387: 25-31. doi:10.1016/j.canlet.2016.05.008

[21] **R. Wahl, H. Jacene, Y. Kasamon, M. Lodge,** "From RECIST to PERCIST: Evolving Considerations for PET Response Criteria in Solid Tumors" 2009 JNM: 50(Suppl 1), 122S-150S. https://dx.doi.org/10.2967/jnumed.108.057307

[22] **K Schmiedehausen,** "NaF PET/CT in Prostate Cancer," White Paper, Siemens Medical Solutions USA, Inc., 2014

[23] **S. Barrington, R. Kluge,** "FDG PET for therapy monitoring in Hodgkin and non-Hodgkin lymphomas," *EJNMMI* (2017) 44(S1): S97-S110.

[24] **V. Vassiliou, D. Andreopoulos, S Frangos , N. Tselis, E. Giannopoulou, S. Lutz.,** "Bone metastases: assessment of therapeutic response through radiological and nuclear medicine imaging modalities" *Clin Oncol (R Coll Radiol)* 2011;23:632–645

[25] **A. Hans Vija, C. Von Gall, P. Ghosh,** "Accurate, reproducible, and standardized quantification," White paper, Siemens Healthineers, 2018

HIGHLIGHTS OF PRESCRIBING INFORMATION

These highlights do not include all the information needed to use Fludeoxyglucose F 18 Injection safely and effectively. See full prescribing information for Fludeoxyglucose F 18 Injection.

Fludeoxyglucose F 18 Injection, USP
For intravenous use
Initial U.S. Approval: 2005

INDICATIONS AND USAGE

Fludeoxyglucose F 18 Injection is indicated for positron emission tomography (PET) imaging in the following settings:

- Oncology: For assessment of abnormal glucose metabolism to assist in the evaluation of malignancy in patients with known or suspected abnormalities found by other testing modalities, or in patients with an existing diagnosis of cancer.
- Cardiology: For the identification of left ventricular myocardium with residual glucose metabolism and reversible loss of systolic function in patients with coronary artery disease and left ventricular dysfunction, when used together with myocardial perfusion imaging.
- Neurology: For the identification of regions of abnormal glucose metabolism associated with foci of epileptic seizures (1).

DOSAGE AND ADMINISTRATION

Fludeoxyglucose F 18 Injection emits radiation. Use procedures to minimize radiation exposure. Screen for blood glucose abnormalities.

- In the oncology and neurology settings, instruct patients to fast for 4 to 6 hours prior to the drug's injection. Consider medical therapy and laboratory testing to assure at least two days of normoglycemia prior to the drug's administration (5.2).
- In the cardiology setting, administration of glucose-containing food or liquids (e.g., 50 to 75 grams) prior to the drug's injection facilitates localization of cardiac ischemia (2.3).

Aseptically withdraw Fludeoxyglucose F 18 Injection from its container and administer by intravenous injection (2).

The recommended dose:

- for adults is 5 to 10 mCi (185 to 370 MBq), in all indicated clinical settings (2.1).
- for pediatric patients is 2.6 mCi in the neurology setting (2.2).

Initiate imaging within 40 minutes following drug injection; acquire static emission images 30 to 100 minutes from time of injection (2).

DOSAGE FORMS AND STRENGTHS

Multi-dose 30mL and 50mL glass vial containing 0.74 to 7.40 GBq/mL (20 to 200 mCi/mL) Fludeoxyglucose F 18 Injection and 4.5mg of sodium chloride with 0.1 to 0.5% w/w ethanol as a stabilizer (approximately 15 to 50 mL volume) for intravenous administration (3).

CONTRAINDICATIONS

None.

WARNINGS AND PRECAUTIONS

- Radiation risks: use smallest dose necessary for imaging (5.1).
- Blood glucose adnormalities: may cause suboptimal imaging (5.2).

ADVERSE REACTIONS

Hypersensitivity reactions have occurred; have emergency resuscitation equipment and personnel immediately available (6).

To report SUSPECTED ADVERSE REACTIONS, contact PETNET Solutions, Inc. at 877-473-8638 or FDA at 1-800-FDA-1088 or www.fda.gov/medwatch.

USE IN SPECIFIC POPULATIONS

- Lactation: Temporarily discontinue breastfeeding. A lactating woman should pump and discard breastmilk for 9 hours after Fludeoxyglucose F 18 Injection (8.2).
- Pediatric Use: Safety and effectiveness in pediatric patients have not been established in the oncology and cardiology settings (8.4).

See 17 for PATIENT COUNSELING INFORMATION

Revised: 10/2019

FULL PRESCRIBING INFORMATION: CONTENTS*

* Sections or subsections omitted from the full prescribing information are not listed.

FULL PRESCRIBING INFORMATION

1 INDICATIONS AND USAGE

Fludeoxyglucose F 18 Injection is indicated for positron emission tomography (PET) imaging in the following settings:

1.1 Oncology

For assessment of abnormal glucose metabolism to assist in the evaluation of malignancy in patients with known or suspected abnormalities found by other testing modalities, or in patients with an existing diagnosis of cancer.

1.2 Cardiology

For the identification of left ventricular myocardium with residual glucose metabolism and reversible loss of systolic function in patients with coronary artery disease and left ventricular dysfunction, when used together with myocardial perfusion imaging.

1.3 Neurology

For the identification of regions of abnormal glucose metabolism associated with foci of epileptic seizures.

2 DOSAGE AND ADMINISTRATION

Fludeoxyglucose F 18 Injection emits radiation. Use procedures to minimize radiation exposure. Calculate the final dose from the end of synthesis (EOS) time using proper radioactive decay factors. Assay the final dose in a properly calibrated dose calibrator before administration to the patient *[see Description (11.2)]*.

2.1 Recommended Dose for Adults

Within the oncology, cardiology and neurology settings, the recommended dose for adults is 5 to 10 mCi (185 to 370 MBq) as an intravenous injection.

2.2 Recommended Dose for Pediatric Patients

Within the neurology setting, the recommended dose for pediatric patients is 2.6 mCi, as an intravenous injection. The optimal dose adjustment on the basis of body size or weight has not been determined *[see Use in Special Populations (8.4)]*.

2.3 Patient Preparation

- To minimize the radiation absorbed dose to the bladder, encourage adequate hydration. Encourage the patient to drink water or other fluids (as tolerated) in the 4 hours before their PET study.
- Encourage the patient to void as soon as the imaging study is completed and as often as possible thereafter for at least one hour.
- Screen patients for clinically significant blood glucose abnormalities by obtaining a history and/or laboratory tests *[see Warnings and Precautions (5.2)]*. Prior to Fludeoxyglucose F 18 PET imaging in the oncology and neurology settings, instruct patient to fast for 4 to 6 hours prior to the drug's injection.
- In the cardiology setting, administration of glucose-containing food or liquids (e.g., 50 to 75 grams) prior to Fludeoxyglucose F 18 Injection facilitates localization of cardiac ischemia.

2.4 Radiation Dosimetry

The estimated human absorbed radiation doses (rem/mCi) to a newborn (3.4 kg), 1-year old (9.8 kg), 5-year old (19 kg), 10-year old (32 kg), 15-year old (57 kg), and adult (70 kg) from intravenous administration of Fludeoxyglucose F 18 Injection are shown in Table 1. These estimates were calculated based on human[2] data and using the data published by the International Commission on Radiological Protection[4] for Fludeoxyglucose ^{18}F. The dosimetry data show that there are slight variations in absorbed radiation dose for various organs in each of the age groups. These dissimilarities in absorbed radiation dose are due to developmental age variations (e.g., organ size, location, and overall metabolic rate for each age group). The identified critical organs (in descending order) across all age groups evaluated are the urinary bladder, heart, pancreas, spleen, and lungs.

Table 1. Estimated Absorbed Radiation Doses (rem/mCi) After Intravenous Administration of Fludeoxyglucose F 18 Injection[a]

Organ	Newborn (3.4 kg)	1-year old (9.8 kg)	5-year old (19 kg)	10-year old (32 kg)	15-year old (57 kg)	Adult (70 kg)
Bladder wall[b]	4.3	1.7	0.93	0.60	0.40	0.32
Heart wall	2.4	1.2	0.70	0.44	0.29	0.22
Pancreas	2.2	0.68	0.33	0.25	0.13	0.096
Spleen	2.2	0.84	0.46	0.29	0.19	0.14
Lungs	0.96	0.38	0.20	0.13	0.092	0.064
Kidneys	0.81	0.34	0.19	0.13	0.089	0.074
Ovaries	0.80	0.8	0.19	0.11	0.058	0.053
Uterus	0.79	0.35	0.19	0.12	0.076	0.062
LLI wall *	0.69	0.28	0.15	0.097	0.060	0.051
Liver	0.69	0.31	0.17	0.11	0.076	0.058
Gallbladder wall	0.69	0.26	0.14	0.093	0.059	0.049
Small intestine	0.68	0.29	0.15	0.096	0.060	0.047
ULI wall **	0.67	0.27	0.15	0.090	0.057	0.046
Stomach wall	0.65	0.27	0.14	0.089	0.057	0.047
Adrenals	0.65	0.28	0.15	0.095	0.061	0.048
Testes	0.64	0.27	0.14	0.085	0.052	0.041
Red marrow	0.62	0.26	0.14	0.089	0.057	0.047
Thymus	0.61	0.26	0.14	0.086	0.056	0.044
Thyroid	0.61	0.26	0.13	0.080	0.049	0.039
Muscle	0.58	0.25	0.13	0.078	0.049	0.039
Bone surface	0.57	0.24	0.12	0.079	0.052	0.041
Breast	0.54	0.22	0.11	0.068	0.043	0.034
Skin	0.49	0.20	0.10	0.060	0.037	0.030
Brain	0.29	0.13	0.09	0.078	0.072	0.070
Other tissues	0.59	0.25	0.13	0.083	0.052	0.042

[a] MIRDOSE 2 software was used to calculate the radiation absorbed dose.
[b] The dynamic bladder model with a uniform voiding frequency of 1.5 hours was used.
* LLI = lower large intestine; ** ULI = upper large intestine

2.5 Radiation Safety – Drug Handling

- Use waterproof gloves, effective radiation shielding, and appropriate safety measures when handling Fludeoxyglucose F 18 Injection to avoid unnecessary radiation exposure to the patient, occupational workers, clinical personnel and other persons.
- Radiopharmaceuticals should be used by or under the control of physicians who are qualified by specific training and experience in the safe use and handling of radionuclides, and whose experience and training have been approved by the appropriate governmental agency authorized to license the use of radionuclides.
- Calculate the final dose from the end of synthesis (EOS) time using proper radioactive decay factors. Assay the final dose in a properly calibrated dose calibrator before administration to the patient *[see Description (11.2)]*.
- The dose of Fludeoxyglucose F 18 used in a given patient should be minimized consistent with the objectives of the procedure, and the nature of the radiation detection devices employed.

2.6 Drug Preparation and Administration

- Calculate the necessary volume to administer based on calibration time and dose.
- Aseptically withdraw Fludeoxyglucose F 18 Injection from its container.
- Inspect Fludeoxyglucose F 18 Injection visually for particulate matter and discoloration before administration, whenever solution and container permit.
- Do not administer the drug if it contains particulate matter or discoloration; dispose of these unacceptable or unused preparations in a safe manner, in compliance with applicable regulations.
- Use Fludeoxyglucose F 18 Injection within 12 hours from the EOS.

2.7 Imaging Guidelines

- Initiate imaging within 40 minutes following Fludeoxyglucose F 18 Injection administration.
- Acquire static emission images 30 to 100 minutes from the time of injection.

3 DOSAGE FORMS AND STRENGTHS

Multiple-dose 30 mL and 50 mL glass vial containing 0.74 to 7.40 GBq/mL (20 to 200 mCi/mL) of Fludeoxyglucose F 18 Injection and 4.5 mg of sodium chloride with 0.1 to 0.5% w/w ethanol as a stabilizer (approximately 15 to 50 mL volume) for intravenous administration.

4 CONTRAINDICATIONS

None.

5 WARNINGS AND PRECAUTIONS

5.1 Radiation Risks

Radiation-emitting products, including Fludeoxyglucose F 18 Injection, may increase the risk for cancer, especially in pediatric patients. Use the smallest dose necessary for imaging and ensure safe handling to protect the patient and health care worker *[see Dosage and Administration (2.5)]*.

5.2 Blood Glucose Abnormalities

In the oncology and neurology setting, suboptimal imaging may occur in patients with inadequately regulated blood glucose levels. In these patients, consider medical therapy and laboratory testing to assure at least two days of normoglycemia prior to Fludeoxyglucose F 18 Injection administration.

6 ADVERSE REACTIONS

Hypersensitivity reactions with pruritus, edema and rash have been reported in the post-marketing setting. Have emergency resuscitation equipment and personnel immediately available.

7 DRUG INTERACTIONS

The interactions of Fludeoxyglucose F 18 Injection with other drugs taken by patients undergoing PET imaging has not been studied.

8 USE IN SPECIFIC POPULATIONS

8.1 Pregnancy

Risk Summary

Data from published case series and case reports describe Fludeoxyglucose F 18 Injection crossing the placenta with uptake by the fetus (see Data). All radiopharmaceuticals have the potential to cause fetal harm depending on the fetal stage of development and the magnitude of the radiation dose. However, published studies that describe Fludeoxyglucose F 18 Injection use in pregnant women have not identified a risk of drug-associated major birth defects, miscarriage, or adverse maternal or fetal outcomes. If considering Fludeoxyglucose F 18 Injection administration to a pregnant woman, inform the patient about the potential for adverse pregnancy outcomes based on the radiation dose from Fludeoxyglucose F 18 Injection and the gestational timing of exposure. The estimated background risk of major birth defects and miscarriage for the indicated population is unknown. All pregnancies have a background risk of birth defect, loss, or other adverse outcomes. In the U.S. general population, the estimated background risk of major birth defects and miscarriage in clinically recognized pregnancies are 2-4% and 15-20%, respectively.

Data

Human Data

Data from published case series and case reports describe Fludeoxyglucose F 18 Injection crossing the placental barrier and visualization of radioactivity throughout the body of the fetus. The estimated fetal absorbed radiation dose from the maximum labeled dose (370 MBq) of Fludeoxyglucose F 18 was 10 mGy with first trimester exposure to PET alone and 20 mGy with first trimester exposure to PET/CT scan combination. Long-term adverse radiation effects to a child exposed to Fludeoyxglucose F 18 Injection in utero are unknown. No adverse fetal effects or radiation-related risks have been identified for diagnostic procedures involving less than 50 mGy, which represents less than 20 mGy fetal doses.

8.2 Lactation

Risk Summary

A published case report and case series show the presence of Fludeoxyglucose F 18 Injection in human milk following administration. There are no data on the effects of Fludeoxyglucose F 18 Injection on the breastfed infant or the effects on milk production. Exposure of Fludeoxyglucose F 18 Injection to a breastfed infant can be minimized by temporary discontinuation of breastfeeding (see Clinical Considerations). The developmental and health benefits of breastfeeding should be considered along with the mother's clinical need for Fludeoxyglucose F 18 Injection, any potential adverse effects on the breastfed child from Fludeoxyglucose F 18 Injection or from the underlying maternal condition.

Clinical Considerations

To decrease radiation exposure to the breastfed infant, advise a lactating woman to pump and discard breastmilk and avoid close (breast) contact with the infant for at least 9 hours after the administration of Fludeoxyglucose F 18 Injection.

8.4 Pediatric Use

The safety and effectiveness of Fludeoxyglucose F 18 Injection in pediatric patients with epilepsy is established on the basis of studies in adult and pediatric patients. In pediatric patients with epilepsy, the recommended dose is 2.6 mCi. The optimal dose adjustment on the basis of body size or weight has not been determined. In the oncology or cardiology settings, the safety and effectiveness of Fludeoxyglucose F 18 Injection have not been established in pediatric patients.

11 DESCRIPTION

11.1 Chemical Characteristics

Fludeoxyglucose F 18 Injection is a positron emitting radiopharmaceutical that is used for diagnostic purposes in conjunction with positron emission tomography (PET) imaging. The active ingredient 2-deoxy-2-[^{18}F]fluoro-D-glucose has the molecular formula of $C_6H_{11}{}^{18}FO_5$ with a molecular weight of 181.26, and has the following chemical structure:

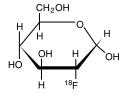

Fludeoxyglucose F 18 Injection is provided as a ready to use sterile, pyrogen free, clear, colorless solution. Each mL contains between 0.740 to 7.40GBq (20.0 to 200 mCi) of 2-deoxy-2-[^{18}F]fluoro-D-glucose at the EOS, 4.5 mg of sodium chloride and 0.1 to 0.5% w/w ethanol as a stabilizer. The pH of the solution is between 4.5 and 7.5. The solution is packaged in a multiple-dose glass vial and does not contain any preservative.

11.2 Physical Characteristics

Fluorine F 18 has a physical half-life of 109.7 minutes and decays to Oxygen O 16 (stable) by positron decay. The principal photons useful for imaging are the dual 511 keV "annihilation" gamma photons, that are produced and emitted simultaneously in opposite direction when the positron interacts with an electron (Table 2).

Table 2. Principal Radiation Emission Data for Fluorine F 18

Radiation/Emission	% Per Disintegration	Mean Energy
Positron (β+)	96.73	249.8 keV
Gamma (±)*	193.46	511.0 keV

*Produced by positron annihilation

From: Kocher, D.C. Radioactive Decay Tables DOE/TIC-I 1026, 89 (1981)

The specific gamma ray constant (point source air kerma coefficient) for fluorine F 18 is 5.7 R/hr/mCi (1.35 x 10^{-6} Gy/hr/kBq) at 1 cm. The half-value layer (HVL) for the 511 keV photons is 4 mm lead (Pb). The range of attenuation coefficients for this radionuclide as a function of lead shield thickness is shown in Table 3. For example, the interposition of an 8 mm thickness of Pb, with a coefficient of attenuation of 0.25, will decrease the external radiation by 75%.

Table 3. Radiation Attenuation of 511 keV Photons by lead (Pb) shielding

Shield thickness (Pb) mm	Coefficient of attenuation
0	0.00
4	0.50
8	0.25
13	0.10
26	0.01
39	0.001
52	0.0001

For use in correcting for physical decay of this radionuclide, the fractions remaining at selected intervals after calibration are shown in Table 4.

Table 4. Physical Decay Chart for Fluorine F 18

Minutes	Fraction Remaining
0*	1.000
15	0.909
30	0.826
60	0.683
110	0.500
220	0.250

*calibration time

12 CLINICAL PHARMACOLOGY

12.1 Mechanism of Action

Fludeoxyglucose F 18 is a glucose analog that concentrates in cells that rely upon glucose as an energy source, or in cells whose dependence on glucose increases under pathophysiological conditions. Fludeoxyglucose F 18 is transported through the cell membrane by facilitative glucose transporter proteins and is phosphorylated within the cell to [^{18}F] FDG-6-phosphate by the enzyme hexokinase. Once phosphorylated it cannot exit until it is dephosphorylated by glucose-6-phosphatase. Therefore, within a given tissue or pathophysiological process, the retention and clearance of Fludeoxyglucose F 18 reflect a balance involving glucose transporter, hexokinase and glucose-6-phosphatase activities. F 18 is used to assess glucose metabolism.

In comparison to background activity of the specific organ or tissue type, regions of decreased or absent uptake of Fludeoxyglucose F 18 reflect the decrease or absence of glucose metabolism. Regions of increased uptake of Fludeoxyglucose F 18 reflect greater than normal rates of glucose metabolism.

12.2 Pharmacodynamics

Fludeoxyglucose F 18 Injection is rapidly distributed to all organs of the body after intravenous administration. After background clearance of Fludeoxyglucose F 18 Injection, optimal PET imaging is generally achieved between 30 to 40 minutes after administration.

In cancer, the cells are generally characterized by enhanced glucose metabolism partially due to (1) an increase in activity of glucose transporters, (2) an increased rate of phosphorylation activity, (3) a reduction of phosphatase activity or, (4) a dynamic alteration in the balance among all these processes. However, glucose metabolism of cancer as reflected by Fludeoxyglucose F 18 accumulation shows considerable variability. Depending on tumor type, stage, and location, Fludeoxyglucose F 18 accumulation may be increased, normal, or decreased. Also, inflammatory cells can have the same variability of uptake of Fludeoxyglucose F 18.

In the heart, under normal aerobic conditions, the myocardium meets the bulk of its energy requirements by oxidizing free fatty acids. Most of the exogenous glucose taken up by the myocyte is converted into glycogen. However, under ischemic conditions, the oxidation of free fatty acids decreases, exogenous glucose becomes the preferred myocardial substrate, glycolysis is stimulated, and glucose taken up by the myocyte is metabolized immediately instead of being converted into glycogen. Under these conditions, phosphorylated Fludeoxyglucose F 18 accumulates in the myocyte and can be detected with PET imaging.

In the brain, cells normally rely on aerobic metabolism. In epilepsy, the glucose metabolism varies. Generally, during a seizure, glucose metabolism increases. Interictally, the seizure focus tends to be hypometabolic.

12.3 Pharmacokinetics

Distribution: In four healthy male volunteers, receiving an intravenous administration of 30 seconds induration, the arterial blood level profile for Fludeoxyglucose F 18 decayed triexponentially. The effective half-life ranges of the three phases were 0.2 to 0.3 minutes, 10 to 13 minutes with a mean and standard deviation (STD) of 11.6 (±) 1.1 min, and 80 to 95 minutes with a mean and STD of 88 (±) 4 min.

Plasma protein binding of Fludeoxyglucose F 18 has not been studied.

Metabolism: Fludeoxyglucose F 18 is transported into cells and phosphorylated to [^{18}F]-FDG-6-phosphate at a rate proportional to the rate of glucose utilization within that tissue. [^{18}F]-FDG-6-phosphate presumably is metabolized to 2-deoxy-2-[^{18}F]fluoro-6-phospho-D-mannose([^{18}F]FDM-6-phosphate).

Fludeoxyglucose F 18 Injection may contain several impurities (e.g., 2-deoxy-2-chloro-D-glucose (ClDG)). Biodistribution and metabolism of ClDG are presumed to be similar to Fludeoxyglucose F 18 and would be expected to result in intracellular formation of 2-deoxy-2-chloro-6-phospho-D-glucose (ClDG-6-phosphate) and 2-deoxy-2-chloro-6-phospho-D-mannose (ClDM-6-phosphate). The phosphorylated deoxyglucose compounds are dephosphorylated and the resulting compounds (FDG, FDM, ClDG, and ClDM) presumably leave cells by passive diffusion. Fludeoxyglucose F 18 and related compounds are cleared from non-cardiac tissues within 3 to 24 hours after administration. Clearance from the cardiac tissue may require more than 96 hours. Fludeoxyglucose F 18 that is not involved in glucose metabolism in any tissue is then excreted in the urine.

Elimination: Fludeoxyglucose F 18 is cleared from most tissues within 24 hours and can be eliminated from the body unchanged in the urine. Within 33 minutes, a mean of 3.9% of the administrated radioactive dose was measured in the urine. The amount of radiation exposure of the urinary bladder at two hours post-administration suggests that 20.6% (mean) of the radioactive dose was present in the bladder.

Special Populations:

The pharmacokinetics of Fludeoxyglucose F 18 Injection have not been studied in renally-impaired, hepatically impaired or pediatric patients. Fludeoxyglucose F 18 is eliminated through the renal system. Avoid excessive radiation exposure to this organ system and adjacent tissues.

The effects of fasting, varying blood sugar levels, conditions of glucose intolerance, and diabetes mellitus on Fludeoxyglucose F 18 distribution in humans have not been ascertained [*see Warnings and Precautions (5.2)*].

13 NONCLINICAL TOXICOLOGY

13.1 Carcinogenesis, Mutagenesis, Impairment of Fertility

Animal studies have not been performed to evaluate the Fludeoxyglucose F 18 Injection carcinogenic potential, mutagenic potential or effects on fertility.

14 CLINICAL STUDIES

14.1 Oncology

The efficacy of Fludeoxyglucose F 18 Injection in positron emission tomography cancer imaging was demonstrated in 16 independent studies. These studies prospectively evaluated the use of Fludeoxyglucose F 18 in patients with suspected or known malignancies, including non-small cell lung cancer, colo-rectal, pancreatic, breast, thyroid, melanoma, Hodgkin's and non-Hodgkin's lymphoma, and various types of metastatic cancers to lung, liver, bone, and axillary nodes. All these studies had at least 50 patients and used pathology as a standard of truth. The Fludeoxyglucose F 18 Injection doses in the studies ranged from 200 MBq to 740 MBq with a median and mean dose of 370 MBq.

In the studies, the diagnostic performance of Fludeoxyglucose F 18 Injection varied with the type of cancer, size of cancer, and other clinical conditions. False negative and false positive scans were observed. Negative Fludeoxyglucose F 18 Injection PET scans do not exclude the diagnosis of cancer. Positive Fludeoxyglucose F 18 Injection PET scans can not replace pathology to establish a diagnosis of cancer. Non-malignant conditions such as fungal infections, inflammatory processes and benign tumors have patterns of increased glucose metabolism that may give rise to false-positive scans. The efficacy of Fludeoxyglucose F 18 Injection PET imaging in cancer screening was not studied.

14.2 Cardiology

The efficacy of Fludeoxyglucose F 18 Injection for cardiac use was demonstrated in ten independent, prospective studies of patients with coronary artery disease and chronic left ventricular systolic dysfunction who were scheduled to undergo coronary revascularization. Before revascularization, patients underwent PET imaging with Fludeoxyglucose F 18 Injection (74 to 370 MBq, 2 to 10 mCi) and perfusion imaging with other diagnostic radiopharmaceuticals. Doses of Fludeoxyglucose F 18 Injection ranged from 74 to 370 MBq (2 to 10 mCi). Segmental, left ventricular, wall-motion assessments of asynergic areas made before revascularization were compared in a blinded manner to assessments made after successful revascularization to identify myocardial segments with functional recovery.

Left ventricular myocardial segments were predicted to have reversible loss of systolic function if they showed Fludeoxyglucose F 18 accumulation and reduced perfusion (i.e., flow-metabolism mismatch). Conversely, myocardial segments were predicted to have irreversible loss of systolic function if they showed reductions in both Fludeoxyglucose F 18 accumulation and perfusion (i.e., matched defects).

Findings of flow-metabolism mismatch in a myocardial segment may suggest that successful revascularization will restore myocardial function in that segment. However, false-positive tests occur regularly, and the decision to have a patient undergo revascularization should not be based on PET findings alone. Similarly, findings of a matched defect in a myocardial segment may suggest that myocardial function will not recover in that segment, even if it is successfully revascularized. However, false-negative tests occur regularly, and the decision to recommend against coronary revascularization, or to recommend a cardiac transplant, should not be based on PET findings alone. The reversibility of segmental dysfunction as predicted with Fludeoxyglucose F 18 PET imaging depends on successful coronary revascularization. Therefore, in patients with a low likelihood of successful revascularization, the diagnostic usefulness of PET imaging with Fludeoxyglucose F 18 Injection is more limited.

14.3 Neurology

In a prospective, open label trial, Fludeoxyglucose F 18 Injection was evaluated in 86 patients with epilepsy. Each patient received a dose of Fludeoxyglucose F 18 Injection in the range of 185 to 370 MBq (5 to 10 mCi). The mean age was 16.4 years (range: 4 months to 58 years; of these, 42 patients were less than 12 years and 16 patients were less than 2 years old). Patients had a known diagnosis of complex partial epilepsy and were under evaluation for surgical treatment of their seizure disorder. Seizure foci had been previously identified on ictal EEGs and sphenoidal EEGs. Fludeoxyglucose F 18 Injection PET imaging confirmed previous diagnostic findings in 16% (14/87) of the patients; in 34% (30/87) of the patients, Fludeoxyglucose F 18 Injection PET images provided new findings. In 32% (27/87), imaging with Fludeoxyglucose F 18 Injection was inconclusive. The impact of these imaging findings on clinical outcomes is not known.

Several other studies comparing imaging with Fludeoxyglucose F 18 Injection results to subsphenoidal EEG, MRI and/or surgical findings supported the concept that the degree of hypometabolism corresponds to areas of confirmed epileptogenic foci. The safety and effectiveness of Fludeoxyglucose F 18 Injection to distinguish idiopathic epileptogenic foci from tumors or other brain lesions that may cause seizures have not been established.

16 HOW SUPPLIED/STORAGE AND DRUG HANDLING

Fludeoxyglucose F 18 Injection is supplied in a multi-dose, capped 30 mL and 50 mL glass vial containing between 0.740 to 7.40 GBq/mL (20 to 200 mCi/mL), of no carrier added 2-deoxy-2-[^{18}F-fluoro-D-glucose, at end of synthesis, in approximately 15 to 50 mL. The contents of each vial are sterile, pyrogen-free and preservative-free.

NDC 40028-511-30; 40028-511-50

Receipt, transfer, handling, possession, or use of this product is subject to the radioactive material regulations and licensing requirements of the U.S. Nuclear Regulatory Commission, Agreement States or Licensing States as appropriate.

Store the Fludeoxyglucose F 18 Injection vial upright in a lead shielded container at 25°C (77°F); excursions permitted to 15-30°C (59-86°F).

Store and dispose of Fludeoxyglucose F 18 Injection in accordance with the regulations and a general license, or its equivalent, of an Agreement State or a Licensing State.

The expiration date and time are provided on the container label. Use Fludeoxyglucose F 18 Injection within 12 hours from the EOS time.

17 PATIENT COUNSELING INFORMATION

Instruct patients in procedures that increase renal clearance of radioactivity. Encourage patients to:

- drink water or other fluids (as tolerated) in the 4 hours before their PET study.
- void as soon as the imaging study is completed and as often as possible thereafter for at least one hour.

Pregnancy: Advise pregnant women of the risk of fetal exposure to radiation with Fludeoxyglucose F 18 Injection [see Use in Specific Populations (8.1)].

Lactation: Advise lactating women that exposure to Fludeoxyglucose F 18 Injection through breast milk can be minimized by pumping and discarding breast milk and avoiding close (breast) contact with the infant for 9 hours after Fludeoxyglucose F 18 Injection [see Use in Specific Populations (8.2)].

Manufactured and distributed by:
PETNET Solutions, Inc.
810 Innovation Drive
Knoxville, TN 37932

PETNET Solutions

Please contact your local Siemens Healthineers sales representative for the most current information or contact one of the addresses listed below. Note: Original images always lose a certain amount of detail when reproduced.

"Siemens Healthineers" is considered a brand name. Its use is not intended to represent the legal entity to which this product is registered. Please contact your local Siemens organization for further details.

All photographs © 2021 Siemens Healthcare GmbH. All rights reserved.

[a] CPU: 4 cores, 64 bit; RAM:>=32 GB
[b] AIDAN platform scanner software version VG80/VJ30
[c] Lesion Scout with Auto ID is not available for sale in the USA and is not commercially available in all countries. Future availability cannot be guaranteed. Please contact your local Siemens Healthineers organization for further details.

Siemens Healthineers Headquarters
Siemens Healthcare GmbH
Henkestr. 127
91052 Erlangen, Germany
Phone: +49 9131 84-0
siemens-healthineers.com

Published by
Siemens Medical Solutions USA, Inc.
Molecular Imaging
2501 North Barrington Road
Hoffman Estates, IL 60192
USA
Phone: +1 847 304-7700
siemens-healthineers.com/mi